Characterization of automotive dampers using higher order frequency response functions

S Cafferty and **G R Tomlinson**
Dynamics Research Group, Department of Mechanical Engineering, University of Sheffield

Abstract: Automotive dampers are an important element of a vehicle's suspension system for controlling road handling and passenger ride comfort. Many automotive dampers have non-linear asymmetric characteristics to accommodate the incompatible requirements between ride comfort and road handling, thus the ride comfort engineer requires techniques that can characterize this non-linear behaviour and provide models of the dampers for use in ride performance simulations of the full suspension system.

The work presented in this paper is concerned with developing a frequency domain technique using higher order frequency response functions (HFRFs) to characterize a Monroe automotive damper. The principal diagonals and multidimensional surfaces of the HFRFs up to third order are obtained. Non-linear damping coefficients for the damper are derived from the HFRFs and the energy transfer properties are investigated.

The results show that the majority of the HFRFs contain no peaks or resonances, indicating that the damper has no preferred frequencies for energy transfer. The accuracy of the damping coefficients determined from the HFRFs is poor. This is due to the inability of the technique to measure the pure HFRFs and separate the effects of non-linearities in the input actuator from those in the damper. It is concluded that these constraints currently impose some limit on the use of the methodology.

Keywords: automotive dampers, non-linear damping, Volterra series, higher order frequency response functions

NOTATION

Overdots denote differentiation with respect to time.

c	damping [N/(m/s)]
$f(t)$	force output (N)
$\hat{f}(t)$	model predicted force output (N)
$f(y, \dot{y})$	restoring force (N)
F	circular frequency (Hz)
ΔF	frequency spacing (Hz)
$H(\omega)$	frequency response function (FRF)
k	stiffness (N/m)
m	mass (kg)
M	number of cycles of input signal
n	number of data points
ΔT	time step (s)
$x(t)$	input excitation force (N)
$X(\omega)$	input force spectrum (N)
$y(t)$	displacement (m)
$\dot{y}(t)$	velocity (m/s)
$\ddot{y}(t)$	acceleration (m/s^2)
$Y(\omega)$	output displacement spectrum (m)
$\Lambda(\omega)$	composite FRF

The MS was received on 24 January 1996 and was accepted for publication on 7 May 1996.

1 INTRODUCTION

The characteristics of the damper are paramount if a vehicle's suspension system is to improve passenger ride comfort and increase vehicle control. The design of an automotive damper requires two optimum damping values, one setting for ride comfort and another 'harder' setting for vehicle control. This incompatibility has led to many automotive dampers having non-linear asymmetric characteristics. The ride comfort engineer requires techniques that can characterize this non-linear behaviour and provide simple models of the damper that can be used in ride performance simulations of the suspension system.

Traditional techniques have adopted a phase plane approach where the force output of the damper is plotted against input displacement (work diagram) and input velocity (characteristic diagram). Recently the restoring force surface (RFS) method has been used to combine the two diagrams to form a three-dimensional surface. This technique is well adapted for the characterization of automotive dampers and has been used successfully (**1**–**4**). The RFS method can represent a wide range of non-linearities but can only display a system's dependency on two variables, namely displacement and velocity. Automotive dampers are known to be frequency dependent.

An alternative technique based on a functional power series known as the Volterra series (**5**) also enables a wide class of non-linear structures to be analysed. The output from a non-linear system is represented by summing the contribution of individual terms in the series. Loosely speaking the coefficients of the terms are known as the Volterra kernels, although these differ from coefficients of normal power series in that they are a function of several variables. By Fourier transforming these kernels the higher order frequency response functions (HFRFs) are obtained. The practical measurement of the Volterra kernels or HFRFs for non-linear systems has become the subject of a considerable amount of research. Bedrosian and Rice (**6**) proposed a technique whereby the Volterra kernels were obtained by multi-sine testing; the technique became known as 'harmonic probing' and is used in this work to obtain the HFRFs up to third order for a Monroe automotive damper from a Volkswagen Passat. The HFRFs are used to derive coefficients for a non-parametric model and investigate the energy transfer properties of the damper.

The layout of the paper is as follows. Section 2 gives a brief theoretical background to the Volterra series, a description of the harmonic probing technique and interpretation of the HFRFs. Section 3 describes the apparatus and Section 4 the experimental procedure. Section 5 discusses the results and Section 6 draws the conclusions from the work.

2 THEORY

2.1 The Volterra series

Only a brief introduction to the Volterra series and interpretation of the HFRFs is presented here. A more detailed description can be found in the references (**7**, **8**).

If an input $X(\omega)$ to a non-linear system produces an output $Y(\omega)$, it can be shown [see reference (**9**)] that

$$Y(\omega) = Y_1(\omega) + Y_2(\omega) + Y_3(\omega) + \cdots + Y_n(\omega) + \cdots \tag{1}$$

Where

$$Y_1(\omega) = H_1(\omega)X(\omega) \tag{2}$$

$$Y_2(\omega) = \frac{1}{2\pi}\int_{-\infty}^{\infty} H_2(\omega_1, \omega - \omega_1)X(\omega_1)X(\omega - \omega_1)\,\mathrm{d}\omega_1 \tag{3}$$

$$Y_3(\omega) = \frac{1}{(2\pi)^2}\int_{-\infty}^{\infty}\int_{-\infty}^{\infty} H_3(\omega_1, \omega_2, \omega - \omega_1 - \omega_2)\cdots X(\omega_1)X(\omega_2)X(\omega - \omega_1 - \omega_2)\,\mathrm{d}\omega_1\,\mathrm{d}\omega_2 \tag{4}$$

$$Y_n(\omega) = \frac{1}{(2\pi)^n}\int_{-\infty}^{\infty}\cdots\int_{-\infty}^{\infty} H_n(\omega_1, \ldots, \omega_{n-1}, \omega - \omega_1, \ldots, \omega_{n-1})X(\omega_1)\cdots X(\omega_{n-1})\cdots X(\omega - \omega_1 - \cdots - \omega_{n-1})\,\mathrm{d}\omega_1\cdots\mathrm{d}\omega_{n-1} \tag{5}$$

The output from the non-linear system is represented by summing the contribution of individual terms in the series. The first term in the series is the contribution from the linear part of the system, the second, third and nth terms represent the quadratic, cubic and nth order contributions to the total output. The terms $H_1, H_2, \ldots, H_n$ in the integrals are known as the *Volterra kernel transforms* or the HFRFs.

2.2 Harmonic probing

Harmonic probing involves exciting a non-linear system with a harmonic input and matching each component in the response spectrum with the corresponding term in the Volterra series. Consider the ideal input of a single harmonic $x(t) = X\mathrm{e}^{i\omega_1 t}$, the output from the system can be represented directly from equation (1) as

$$y(t) = XH_1(\omega_1)\,\mathrm{e}^{i\omega_1 t} + X^2 H_2(\omega_1, \omega_1)\,\mathrm{e}^{i2\omega_1 t} + X^3 H_3(\omega_1, \omega_1, \omega_1)\,\mathrm{e}^{i3\omega_1 t} + \cdots + X^n H_n(\omega_1, \ldots, \omega_1)\,\mathrm{e}^{in\omega_1 t} + \cdots \tag{6}$$

The series contains an infinite number of terms at discrete integer multiples of the fundamental frequency ω_1. Each term represents a harmonic that would be seen in the output spectrum if a one-dimensional Fourier transform was applied to the response data. By relating each individual harmonic with its corresponding term in the Volterra series the HFRFs can be determined. For example, if the second harmonic $Y(2\omega_1)$ in the output response was measured, the second order FRF can be obtained from

$$H_2(\omega_1, \omega_1) = \frac{Y(2\omega_1)}{X^2} \tag{7}$$

If ω_1 was stepped over a range of frequencies and the FRF computed at each frequency step, the 'principal diagonal' of the second-order FRF would be obtained.

To explain the meaning of 'principal diagonal' it is necessary to recognize that FRFs higher than first order are multidimensional Fourier transforms of the Volterra kernels, where the number of dimensions required to characterize them completely is equal to the order of FRF. Thus in the current example, to characterize fully the second-order FRF $H_2(\omega_1, \omega_2)$, the input must be composed of two harmonics both stepped over the frequency range to produce the full multidimensional FRF surface. Similarly, to express fully the nth order FRF, would require the input of n harmonics all stepped over the frequency range. Therefore, by using a single harmonic, one is effectively reducing the multi-dimensionality of the HFRF to a single

dimension and probing along a line in the surface where the frequency of all the input harmonics are equal, i.e. $\omega_1 = \omega_2 = \omega_3 = \omega_n$.

2.3 Harmonic probing with a sinusoidal input

By probing with a single harmonic input it is possible to acquire the exact Volterra kernels and hence the pure HFRFs for a non-linear system. Unfortunately, it is not possible to generate a pure harmonic as an excitation signal. The nearest physical signal available is a sine wave, i.e. $x(t) = X\cos(\omega_1 t)$. A sine wave contains two harmonics

$$x(t) = \frac{X}{2}(e^{i\omega_1 t} + e^{-i\omega_1 t}) \tag{8}$$

The inclusion of the extra harmonic produces additional terms in the Volterra series representation of the output response. These terms can interact and create additional components to the harmonics in the output spectrum.

The response of a non-linear system to a single sine wave can be written from equation (1) as

$$\begin{aligned} y(t) = {} & H_1(\omega_1)\left(\frac{X}{2}\right)e^{i\omega_1 t} + H_1(-\omega_1)\left(\frac{X}{2}\right)e^{-i\omega_1 t} \\ & + H_2(\omega_1, \omega_1)\left(\frac{X}{2}\right)^2 e^{i2\omega_1 t} \\ & + H_2(-\omega_1, -\omega_1)\left(\frac{X}{2}\right)^2 e^{-i2\omega_1 t} \\ & + H_2(\omega_1, -\omega_1)\left(\frac{X}{2}\right)^2 + H_2(-\omega_1, \omega_1)\left(\frac{X}{2}\right)^2 \\ & + H_3(\omega_1, \omega_1, \omega_1)\left(\frac{X}{2}\right)^3 e^{i3\omega_1 t} \\ & + H_3(-\omega_1, -\omega_1, -\omega_1)\left(\frac{X}{2}\right)^3 e^{-i3\omega_1 t} \\ & + H_3(\omega_1, \omega_1, -\omega_1)\left(\frac{X}{2}\right)^3 e^{i\omega_1 t} \\ & + H_3(-\omega_1, -\omega_1, \omega_1)\left(\frac{X}{2}\right)^3 e^{-i\omega_1 t} \\ & + H_3(\omega_1, -\omega_1, \omega_1)\left(\frac{X}{2}\right)^3 e^{i\omega_1 t} \\ & + H_3(-\omega_1, \omega_1, -\omega_1)\left(\frac{X}{2}\right)^3 e^{-i\omega_1 t} \\ & + H_3(-\omega_1, \omega_1, \omega_1)\left(\frac{X}{2}\right)^3 e^{i\omega_1 t} \\ & + H_3(\omega_1, -\omega_1, -\omega_1)\left(\frac{X}{2}\right)^3 e^{-i\omega_1 t} \\ & + \text{higher order terms} \end{aligned} \tag{9}$$

It can be shown from reference (**10**) that the kernel transforms can be assumed symmetrical, i.e. $H_2(\omega_1, \omega_2) = H_2(\omega_2, \omega_1)$ and the expression can therefore be simplified to

$$\begin{aligned} y(t) = {} & H_1(\omega_1)\left(\frac{X}{2}\right)e^{i\omega_1 t} + H_1(-\omega_1)\left(\frac{X}{2}\right)e^{-i\omega_1 t} \\ & + H_2(\omega_1, \omega_1)\left(\frac{X}{2}\right)^2 e^{i2\omega_1 t} \\ & + H_2(-\omega_1, -\omega_1)\left(\frac{X}{2}\right)^2 e^{-i2\omega_1 t} \\ & + 2H_2(\omega_1, -\omega_1)\left(\frac{X}{2}\right)^2 \\ & + H_3(\omega_1, \omega_1, \omega_1)\left(\frac{X}{2}\right)^3 e^{i3\omega_1 t} \\ & + H_3(-\omega_1, -\omega_1, -\omega_1)\left(\frac{X}{2}\right)^3 e^{-i3\omega_1 t} \\ & + 3H_3(\omega_1, \omega_1, -\omega_1)\left(\frac{X}{2}\right)^3 e^{i\omega_1 t} \\ & + 3H_3(-\omega_1, -\omega_1, \omega_1)\left(\frac{X}{2}\right)^3 e^{-i\omega_1 t} \\ & + \ldots \text{higher order terms} \end{aligned} \tag{10}$$

Using the property of conjugate symmetry for a complex quantity z, i.e.

$$z\,e^{i\omega t} + z^*\,e^{-i\omega t} = 2|z|\cos(\omega t + \angle z)$$

the series finally becomes

$$\begin{aligned} y(t) = {} & X|H_1(\omega_1)|\cos[\omega_1 t + \angle H_1(\omega_1)] \\ & + \frac{1}{2}X^2|H_2(\omega_1, \omega_1)|\cos[2\omega_1 t + \angle H_2(\omega_1, \omega_1)] \\ & + \frac{1}{2}X^2|H_2(\omega_1, -\omega_1)| \end{aligned}$$

$$+\frac{1}{4}X^3|H_3(\omega_1, \omega_1, \omega_1)|\cos$$

$$\times[3\omega_1 t + \angle H_3(\omega_1, \omega_1, \omega_1)]$$

$$+\frac{3}{4}X^3|H_3(\omega_1, \omega_1, -\omega_1)|\cos$$

$$\times[\omega_1 t + \angle H_3(\omega_1, \omega_1, -\omega_1)]$$

$$+ \text{higher order terms} \tag{11}$$

The first harmonic at ω_1 contains an additional component due to the third-order FRF $H_3(\omega_1, \omega_1, -\omega_1)$ term. If the series was extended to infinity, the first harmonic would also contain components from $H_5(\omega_1, \omega_1, \omega_1, -\omega_1, -\omega_1)$, $H_7(\omega_1, \omega_1, \omega_1, \omega_1, -\omega_1, -\omega_1, -\omega_1)$ and all odd ordered terms where the combination of positive and negative values for ω total ω_1. Similarly, the second harmonic will contain components from the fourth-order FRF $H_4(\omega_1, \omega_1, \omega_1, -\omega_1)$, and all even ordered terms higher than second order where the addition of the positive and negative values for ω total $2\omega_1$. This process of higher order terms producing additional components to lower order harmonics will affect all harmonics in the output spectrum. The contribution of each additional term to the harmonic will depend not only on the amplitude of the term but also on the phase difference between itself and the first term in the series.

When measuring harmonics in the response spectrum it is impossible to separate the individual components that make up a harmonic. Therefore, the true Volterra kernels and hence the pure HFRFs can no longer be determined. To account for the extra terms the measurable HFRFs will be referred to as composite HFRFs and denoted $\Lambda_1, \Lambda_2, \ldots, \Lambda_n$ to represent the first, second ... nth-order FRF. Composite HFRFs are therefore dependent on the type and level of excitation.

These additional terms are usually called 'degenerate' terms because they tend to corrupt or distort the composite HFRFs especially around the fundamental resonance and at high excitation levels. To illustrate the type of distortion, Fig. 1 shows the principal diagonal of the first three pure HFRFs in terms of receptance for the system

$$m\ddot{y}(t) + c\dot{y}(t) + k_1 y(t) + k_2 y(t)^2 + k_3 y(t)^3 = x(t) \tag{12}$$

with the parameters

$m = 1.0$ kg

$c = 5.0$ N/(m/s)

$k_1 = 10^4$ N/m

$k_2 = 10^7$ N/m^2

$k_3 = 5 \times 10^9$ N/m^3

The system's response up to third order to a single harmonic of unit amplitude can be written directly from equation (6) as

$$y(t) = H_1(\omega)\,e^{i\omega t} + H_2(\omega, \omega)\,e^{i2\omega t} + H_3(\omega, \omega, \omega)\,e^{i3\omega t} \tag{13}$$

Differentiating equation (13) for the velocity and acceleration gives

$$\dot{y}(t) = i\omega H_1(\omega)\,e^{i\omega t} + i2\omega H_2(\omega, \omega)\,e^{i2\omega t} + i3\omega H_3(\omega, \omega, \omega)\,e^{i3\omega t} \tag{14}$$

$$\ddot{y}(t) = -\omega^2 H_1(\omega)\,e^{i\omega t} - (2\omega)^2 H_2(\omega, \omega)\,e^{i2\omega t} - (3\omega)^2 H_3(\omega, \omega, \omega)\,e^{i3\omega t} \tag{15}$$

Substituting y, $\dot{y}$ and $\ddot{y}$ in to equation (12) and equating coefficients of $e^{i\omega t}$, $e^{i2\omega t}$ and $e^{i3\omega t}$ gives expressions for the first-, second- and third-order FRF respectively,

$$H_1(\omega) = \frac{1}{(k_1 - m\omega^2) + ic\omega} \tag{16}$$

$$H_2(\omega, \omega) = \frac{-k_2 H_1(\omega) H_1(\omega)}{[k_1 - m(2\omega)^2] + ic2\omega} = -H_1(2\omega) k_2 H_1(\omega)^2 \tag{17}$$

$$H_3(\omega, \omega, \omega) = \frac{-2k_2 H_1(\omega) H_2(\omega, \omega) - k_3 H_1(\omega) H_1(\omega) H_1(\omega)}{[k_1 - m(3\omega)^2] + ic3\omega}$$

$$= -H_1(3\omega)[2k_2 H_1(\omega) H_2(\omega, \omega) + k_3 H_1(\omega)^3]$$

$$= 2k_2^2 H_1(3\omega) H_1(2\omega) H_1(\omega)^3 - k_3 H_1(3\omega) H_1(\omega)^3 \tag{18}$$

The first-order FRF is unaffected by the non-linear parameters and is simply determined by the linear part of the system. The magnitude of the FRF contains a single peak at a resonant frequency $\omega_r = 15.9$ Hz and a corresponding phase change of 180° centred around the resonance. At low frequency the magnitude asymptotes to

$$\frac{1}{k_1} = 10^{-4} \text{ m/N}$$

Equations (17) and (18) show how HFRFs can be expressed in terms of lower order FRFs and ultimately $H_1(\omega)$. As a consequence the resonances of the HFRFs are determined by the first-order resonance. The second-order FRF contains a primary resonance at ω_r because of the term $H_1(\omega)^2$ and a secondary resonance at $\omega_r/2 = 7.95$ Hz because of the $H_1(2\omega)$ term. The phase change associated with the

secondary resonance is 180°, where the primary resonance now has a phase change of 360° because the term $H_1(\omega)$ is raised to the power 2. At low frequency the magnitude of the second-order FRF asymptotes to

$$\frac{k_2}{k_1^3} = 10^{-5}\ \mathrm{m/N^2}$$

The third-order FRF contains the primary and secondary resonances and a third resonance at $\omega_r/3 = 5.3$ Hz because of the $H_1(3\omega)$ term. The phase change associated with the primary resonance is now 540° because the $H_1(\omega)$ term is raised to the power 3. At low frequency the magnitude asymptotes to

$$\frac{2k_2^2}{k_1^5} - \frac{k_3}{k_1^4} = 1.5 \times 10^{-6}\ \mathrm{m/N^3}$$

These results show how the characteristics of a non-linear system can be identified from the pure HFRFs.

A numerical simulation routine was written to perform a stepped sine test emulating the procedure that would be adopted in testing a real structure to obtain the composite HFRFs for the system given by equation (12). The response of the system was integrated using a fourth-order Runge–Kutta routine. At each frequency step the sampling frequency was set to 16 times the frequency of interest to ensure aliasing was avoided. For each simulation a number of 'run up' points, equivalent to 60 s of data, was generated to ensure all transients had decayed before one complete cycle of input force and output displacement data was recorded. A conventional fast Fourier transform (FFT) routine was applied to the data and the first three composite HFRFs computed from the spectra information. The input frequency was then incremented and the procedure repeated. The composite HFRFs were computed over a frequency range of 4–20 Hz with a 0.05 Hz increment step. The simulation was repeated for input amplitude levels of 0.1, 0.3, 0.5, 0.7, and 0.9 N peak.

Figure 2 shows the principal diagonals of the first three composite HFRFs in terms of receptance for the system given by equation (12). As the amplitude of the input is increased, the distortion effectively skews the fundamental resonance on all the HFRFs to a lower frequency, an effect known as 'softening' due to the large quadratic term in the system. At high input amplitudes above 0.6 N, the first-order composite FRF also begins to distort at 7.95 Hz; this is due to the degenerate third-order term $H_3(\omega, \omega, -\omega)$ containing a second-order H_2 function at 2ω, i.e.

$$H_3(\omega, \omega, -\omega) = H_1(\omega)\left\{-\frac{2}{3}k_2[2H_1(\omega)H_2(\omega, -\omega) + H_1(-\omega)H_2(\omega, \omega)]\right\} \ldots - k_3 H_1(\omega)H_1(\omega)H_1(-\omega) \quad (19)$$

where

$$H_2(\omega, \omega) = -k_2 H_1(2\omega)H_1(\omega)H_1(\omega) \quad (20)$$

The existence of the HFRFs depends on the type of non-linearity within a system; the system defined by equation (12) contained both a quadratic and cubic stiffness which produced components in the second- and third-order FRFs, indeed all HFRFs would exist for this system. However, if the system contained only a non-linear cubic term, i.e. $k_2 = 0$, all components in the second-order FRF would be null and the third-order FRF would be modified, containing only two resonances at ω_r and $\omega_r/3$. The first-order FRF would be unchanged. Therefore for all even-ordered FRFs to exist, a non-linear system must contain an even-ordered non-linear parameter. However, a non-linear system containing only first- and second-order terms will still produce all odd-ordered FRFs because of the first-order term.

The form of distortion on the composite HFRFs is also dependent on the type of non-linearity within a system. If a system contained only a positive non-linear cubic term the distortion would skew the fundamental resonance to a higher frequency, an effect known as 'hardening'.

Comparison of Figs 1 and 2 shows that the effect of the degenerate terms becomes more significant as the input amplitude is increased. At low amplitudes the composite HFRFs appear to contain no distortion, in effect they converge to the true Volterra kernel transforms obtained previously from probing with a single harmonic.

2.4 Multidimensional HFRFs

To derive expressions for the second-order multidimensional FRF for the system given by equation (12) the input must contain two harmonics

$$x(t) = X_1 e^{i\omega_1 t} + X_2 e^{i\omega_2 t} \quad (21)$$

From equation (6) the response can be written

$$y(t) = H_1(\omega_1)X_1 e^{i\omega_1 t} + H_1(\omega_2)X_2 e^{i\omega_2 t} + H_2(\omega_1, \omega_1)X_1^2 e^{i2\omega_1 t} + H_2(\omega_2, \omega_2)X_2^2 e^{i2\omega_2 t} + 2H_2(\omega_1, \omega_2)X_1 X_2 e^{i(\omega_1+\omega_2)t} + \text{higher order terms} \quad (22)$$

Substituting expressions for y, $\dot{y}$ and $\ddot{y}$ into equation (12) and equating coefficients of $X_1 X_2 e^{i(\omega_1+\omega_2)t}$ gives

$$H_2(\omega_1, \omega_2) = \frac{-k_2 H_1(\omega_1)H_1(\omega_2)}{k_1 - m(\omega_1+\omega_2)^2 + ic(\omega_1+\omega_2)} \quad (23)$$

which can be reduced to

$$H_2(\omega_1, \omega_2) = -k_2 H_1(\omega_1)H_1(\omega_2)H_1(\omega_1+\omega_2) \quad (24)$$

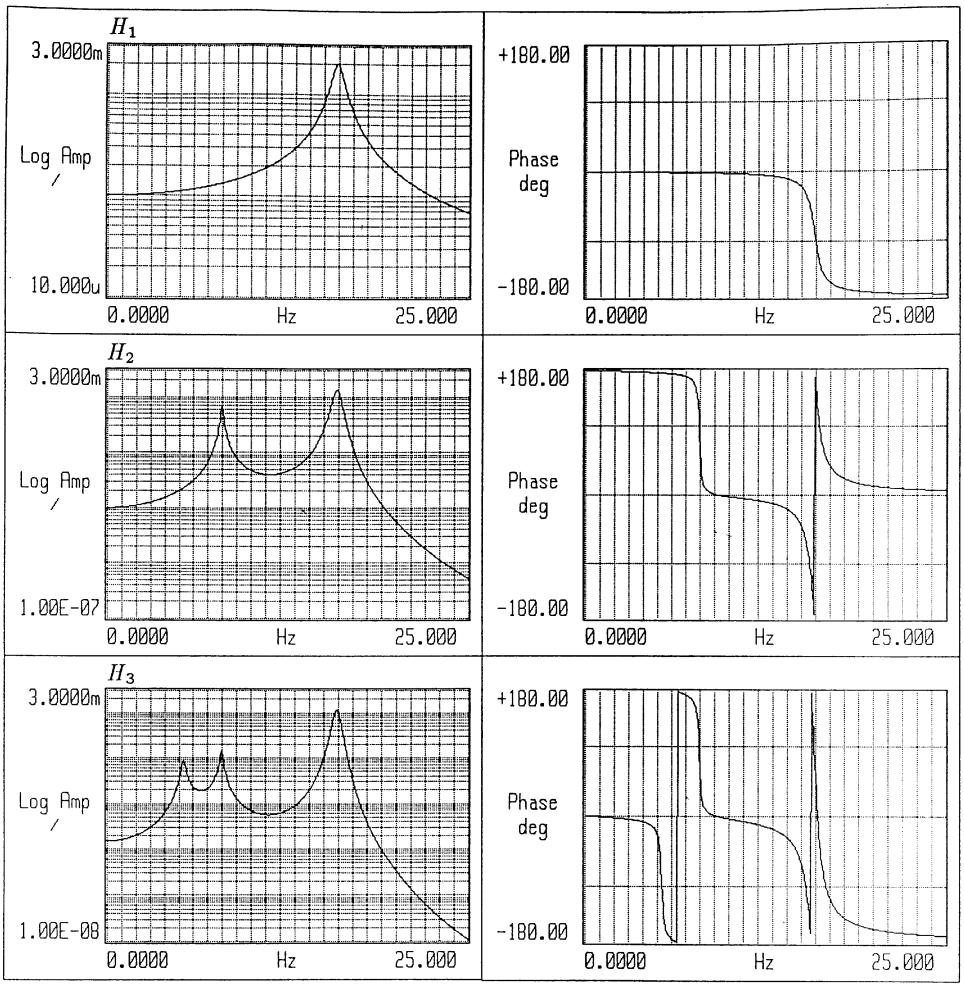

Fig. 1 The principal diagonals of the first-, second- and third-order receptance FRFs for the system $\ddot{y}(t) + 5\dot{y}(t) + 10^4 y(t) + 10^7 y(t)^2 + 5.0 \times 10^9 y(t)^3 = x(t)$

Figure 3 shows the principal quadrant ($\omega_1 > 0$, $\omega_2 > 0$) of the second-order FRF $H_2(\omega_1, \omega_2)$ in terms of gain and phase and corresponding contour plots for the system over the frequency range 0–25 Hz with a 1 N peak input. Clearly the FRF is symmetrical about the line where $\omega_1 = \omega_2$, the principal diagonal. If ω_r denotes the fundamental resonance of the system at 15.9 Hz, three peaks can be observed in the magnitude plot at points where $\omega_1 = \omega_r$ and $\omega_2 = 0$, $\omega_1 = 0$ and $\omega_2 = \omega_r$, and $\omega_1 = \omega_2 = \omega_r$. The three peaks are connected by ridges; these ridges are important in determining the energy transfer properties of the system. The ridge that runs along the line where $\omega_1 + \omega_2 = \omega_r$ characterizes the energy transfer that occurs when any two harmonics are at frequencies which sum to the fundamental resonant frequency, thus exciting the resonance. This can be important in some situations, for example when the input is a broadband random signal, if the second-order FRF exists then any two pairs of harmonics can combine to excite the fundamental resonance even if the input is band-limited to a frequency range which does not include the resonance. In theory the second-order FRF is defined for all frequencies and is therefore not restricted to the principal quadrant and can describe any interaction which can take place between any two positive or negative frequencies.

To define the multidimensional third-order FRF $H_3(\omega_1, \omega_2, \omega_3)$ for the system, the input must contain three individual harmonics, i.e.

$$x(t) = X_1 e^{i\omega_1 t} + X_2 e^{i\omega_2 t} + X_3 e^{i\omega_3 t} \tag{25}$$

From equation (6) the response can be written as

$$\begin{aligned} y(t) = {} & H_1(\omega_1)X_1 e^{i\omega_1 t} + H_1(\omega_2)X_2 e^{i\omega_2 t} \\ & + H_1(\omega_3)X_3 e^{i\omega_3 t} \\ & + H_2(\omega_1, \omega_1)X_1^2 e^{i2\omega_1 t} + H_2(\omega_2, \omega_2)X_2^2 e^{i2\omega_2 t} \\ & + H_2(\omega_3, \omega_3)X_3^2 e^{i2\omega_3 t} \\ & + 2H_2(\omega_1, \omega_2)X_1 X_2 e^{i(\omega_1+\omega_2)t} \end{aligned}$$

$$
\begin{aligned}
&+ 2H_2(\omega_2, \omega_3)X_2X_3\, e^{i(\omega_2+\omega_3)t} \\
&+ 2H_2(\omega_1, \omega_3)X_1X_3\, e^{i(\omega_1+\omega_3)t} \\
&+ H_3(\omega_1, \omega_1, \omega_1)X_1^3\, e^{i3\omega_1 t} \\
&+ H_3(\omega_2, \omega_2, \omega_2)X_2^3\, e^{i3\omega_2 t} \\
&+ H_3(\omega_3, \omega_3, \omega_3)X_3^3\, e^{i3\omega_3 t} \\
&+ 3H_3(\omega_1, \omega_1, \omega_2)X_1^2X_2\, e^{i(2\omega_1+\omega_2)t} \\
&+ 3H_3(\omega_1, \omega_2, \omega_2)X_1X_2^2\, e^{i(\omega_1+2\omega_2)t} \\
&+ 3H_3(\omega_2, \omega_2, \omega_3)X_2^2X_3\, e^{i(2\omega_2+\omega_3)t} \\
&+ 3H_3(\omega_2, \omega_3, \omega_3)X_2X_3^2\, e^{i(\omega_2+2\omega_3)t} \\
&+ 3H_3(\omega_1, \omega_1, \omega_3)X_1^2X_3\, e^{i(2\omega_1+\omega_3)t} \\
&+ 3H_3(\omega_1, \omega_3, \omega_3)X_1X_3^2\, e^{i(\omega_1+2\omega_3)t} \\
&+ 6H_3(\omega_1, \omega_2, \omega_3)X_1X_2X_3\, e^{i(\omega_1+\omega_2+\omega_3)t} \\
&+ \text{higher order terms} \qquad (26)
\end{aligned}
$$

and must contain all terms up to third order. Substituting expressions for y, $\dot{y}$ and $\ddot{y}$ into equation (2) and equating coefficients of $X_1X_2X_3\, e^{i(\omega_1+\omega_2+\omega_3)t}$ gives an expression for the third-order FRF,

$$
\begin{aligned}
H_3(\omega_1, \omega_2, \omega_3) = \\
H_1(\omega_1, \omega_2, \omega_3)\Big\{ &-\frac{2k_2}{3}[H_1(\omega_1)H_2(\omega_2, \omega_3) \\
&+ H_1(\omega_2)H_2(\omega_1, \omega_3) \cdots + H_1(\omega_3)H_2(\omega_1, \omega_2)] \\
&- k_3 H_1(\omega_1)H_1(\omega_2)H_1(\omega_3)\Big\} \qquad (27)
\end{aligned}
$$

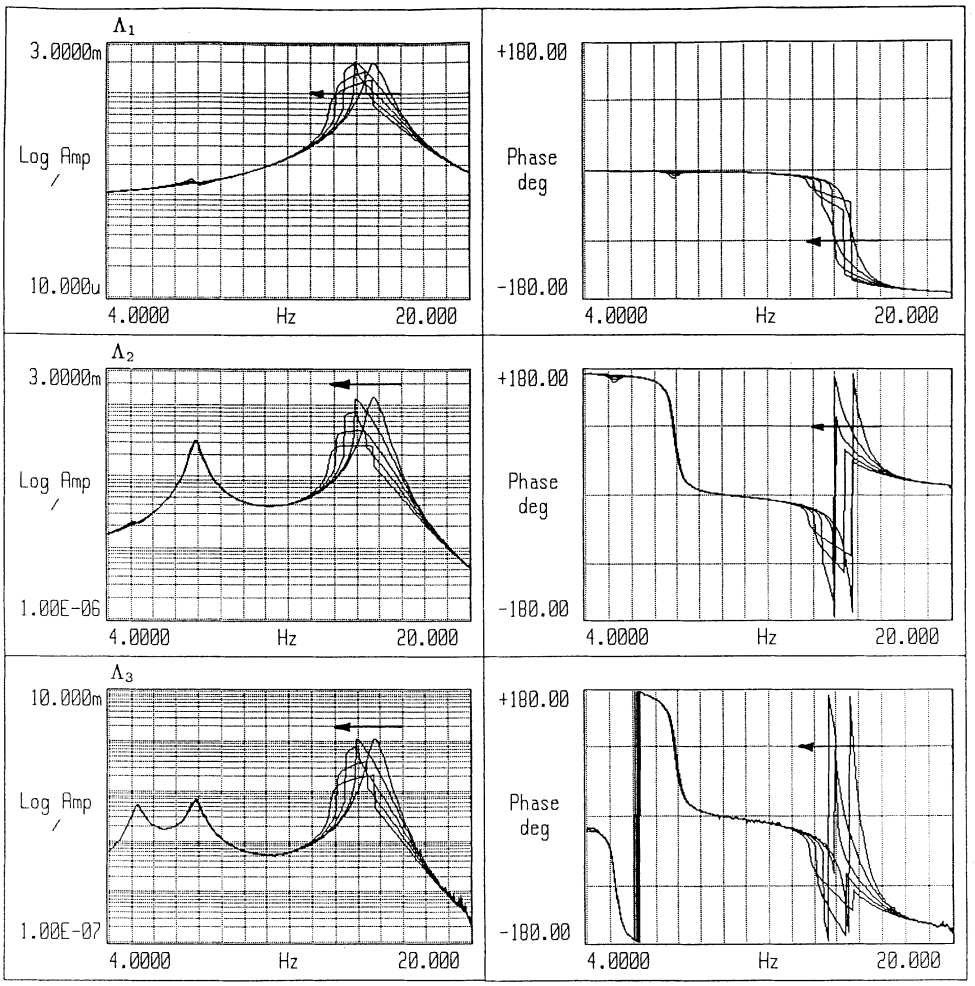

Fig. 2 The principal diagonals of the first-, second- and third-order receptance FRFs for the system $\ddot{y}(t) + 5\dot{y}(t) + 10^4 y(t) + 10^7 y(t)^2 + 5 \times 10^9 y(t)^3 = x(t)$ showing how degenerate terms effect the FRF

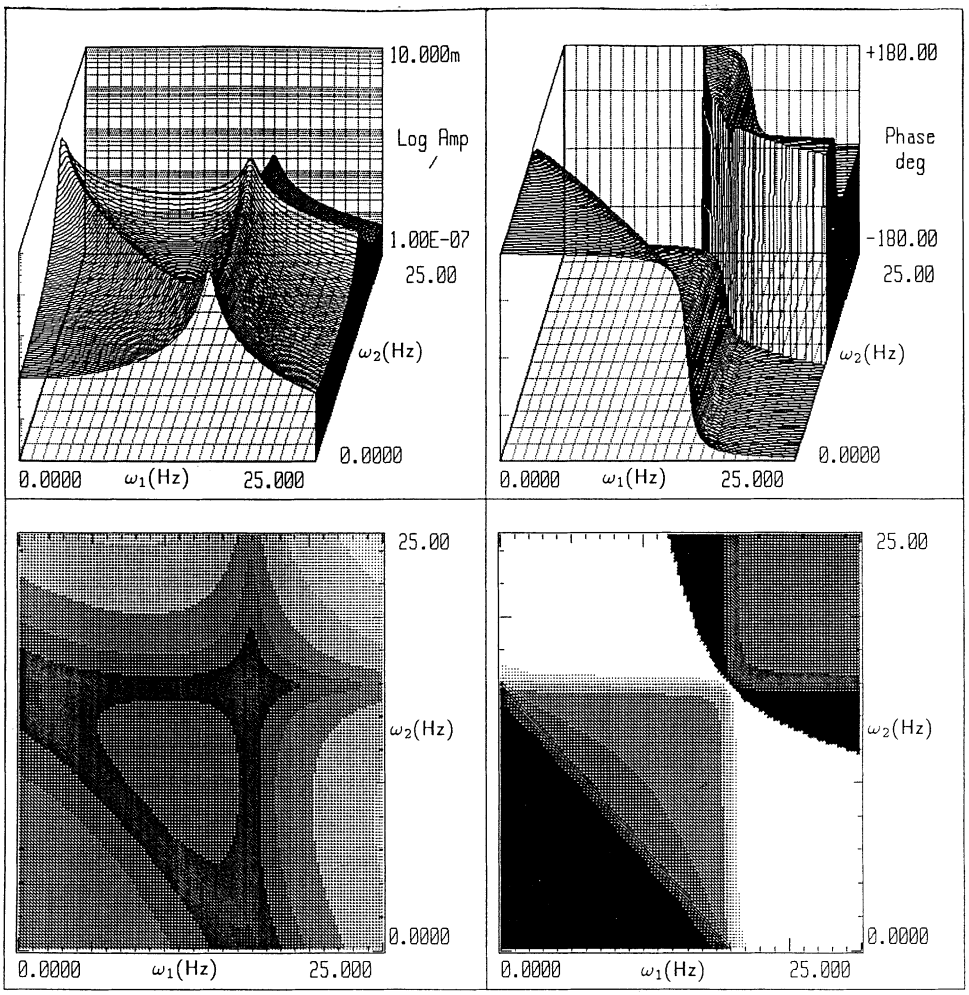

Fig. 3 The principal quadrant of the FRF $H_2(\omega_1, \omega_2)$ for the system $\ddot{y}(t) + 5\dot{y}(t) + 10^4 y(t) + 10^7 y(t)^2 + 5 \times 10^9 y(t)^3 = x(t)$

which can be written in terms of H_1,

$$H_3(\omega_1, \omega_2, \omega_3) = H_1(\omega_1, \omega_2, \omega_3)\left\{\frac{2k_2^2}{3}[H_1(\omega_1)H_1(\omega_2)H_1(\omega_3)H_1(\omega_2+\omega_3) + H_1(\omega_2)H_1(\omega_1)H_1(\omega_3)H_1(\omega_1+\omega_3) + H_1(\omega_3)H_1(\omega_1)H_1(\omega_2)H_1(\omega_1+\omega_2)] - k_3 H_1(\omega_1)H_1(\omega_2)H_1(\omega_3)\right\} \quad (28)$$

The multidimensional third-order FRF $H_3(\omega_1, \omega_2, \omega_3)$ describes the interactions that can take place between any three harmonics. To represent the FRF fully requires three independent frequency axes and four dimensions if the magnitude or phase is to be illustrated. Clearly such a plot is difficult to visualize. To overcome this, the FRF is normally only probed in the plane $(\omega_1, \omega_2, \omega_1)$, effectively taking a slice through the complete FRF along the plane where $\omega_3 = \omega_1$. This slice is easily represented in three-dimensional space allowing the gain and phase information to be interpreted.

Figure 4 shows the principal quadrant of $H_3(\omega_1, \omega_2, \omega_1)$ for the system given by equation (12) over the range of 0–25 Hz with an input level = 1 N peak. The HFRF is no longer symmetrical in the frequency axis and with the relatively large number of local peaks in the magnitude plot, it is difficult to interpret. If ω_r defines the fundamental resonance at 15.9 Hz there are ridges where

$\omega_1 = \omega_r$ from the term $H_1(\omega_1)$

$\omega_2 = \omega_r$ from the term $H_1(\omega_2)$

$2\omega_1 = \omega_r$ from the term $H_1(\omega_1 + \omega_3)$

$\omega_1 + \omega_2 = \omega_r$ from the term $H_1(\omega_1 + \omega_2)$ and $H_1(\omega_2 + \omega_3)$

$2\omega_1 + \omega_2 = \omega_r$ from the term $H_1(\omega_1 + \omega_2 + \omega_3)$

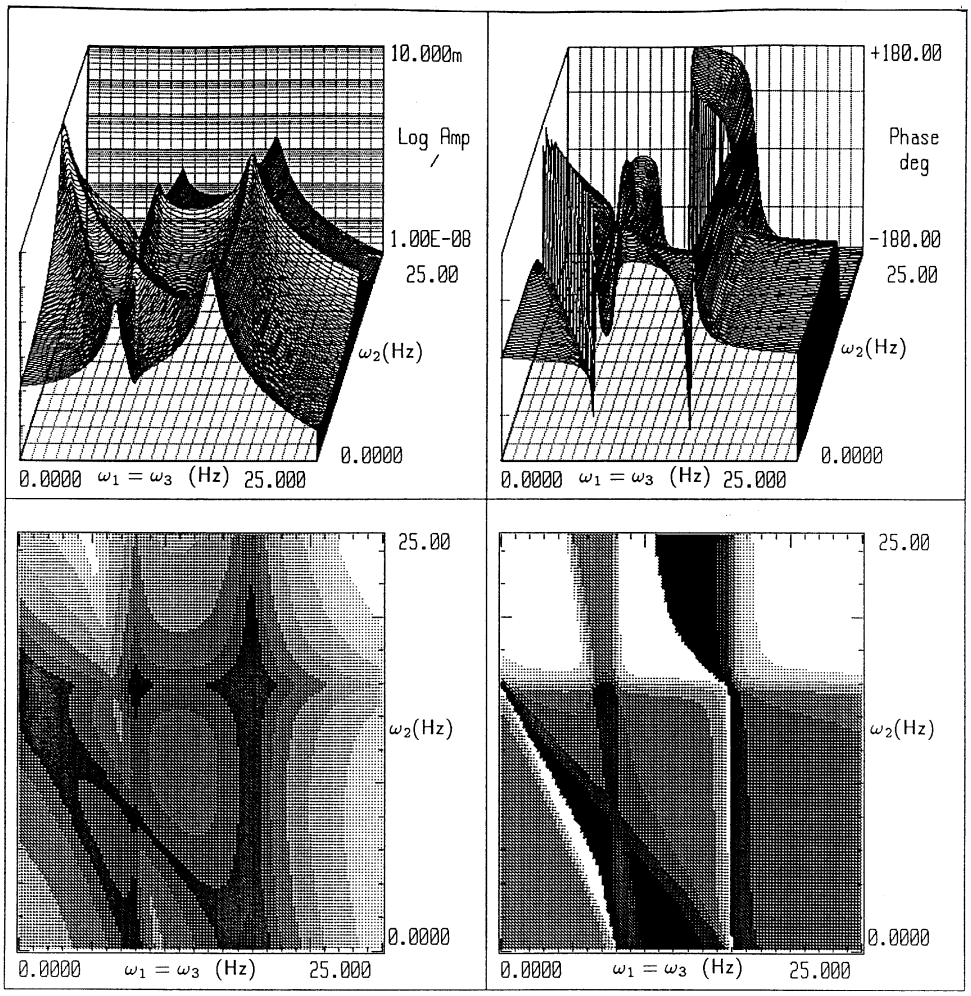

Fig. 4 The principal quadrant of the FRF $H_3(\omega_1, \omega_2, \omega_1)$ for the system $\ddot{y}(t) + 5\dot{y}(t) + 10^4 y(t) + 10^7 y(t)^2 + 5 \times 10^9 y(t)^3 = x(t)$

Unfortunately the multidimensional HFRFs suffer from the same problems as the principal diagonals when the physical input of a sine wave is used. The use of a sine wave input not only produces degenerate terms that skew the resonant peaks of the HFRF, but the additional terms can also produce ridges on the surfaces when the two input frequencies are multiples of each other. For example, Fig. 5 shows the output spectrum from a non-linear system (whose second- and third-order FRFs exist) for an input of two sine waves at 20 and 17 Hz, 20 and 10 Hz, and both at 20 Hz. Tables 1, 2 and 3 show the corresponding frequency components produced in the Volterra series response, assuming terms higher than third order are negligible for the three sets of frequencies.

Clearly when the two frequencies are not multiples of each other, the second-order harmonic at 37 Hz has no additional components contributing to it. However, when the two frequencies are 20 and 10 Hz the second-order harmonic at 30 Hz now has two extra components from the third-order terms. Similarly when the two input frequencies are equal at 20 Hz, the second-order harmonic at 40 Hz contains two extra components from the second-order terms.

These extra components that occur when the two input frequencies are multiples of each other produce additional ridges on the surface of the multidimensional HFRFs. Figure 6 shows the principal quadrant of the composite second-order FRF in terms of gain and phase and corresponding contour plots for the system given by equation (12). Clearly a ridge can now be seen along the principal diagonal in the magnitude plot due to the additional components of the second-order harmonic when the two frequencies are equal. The additional components to the second-order harmonic from the third-order terms are clearly negligible, or there would be ridges along the lines where $\omega_1 = \omega_2/2$ and $\omega_2 = \omega_1/2$. To overcome this problem Boyd (**11**) suggested the rather limiting technique of using frequencies that are prime numbers. However, in this research, a linear interpolation between the frequency points where the ridges occur is used, effectively smoothing the FRF.

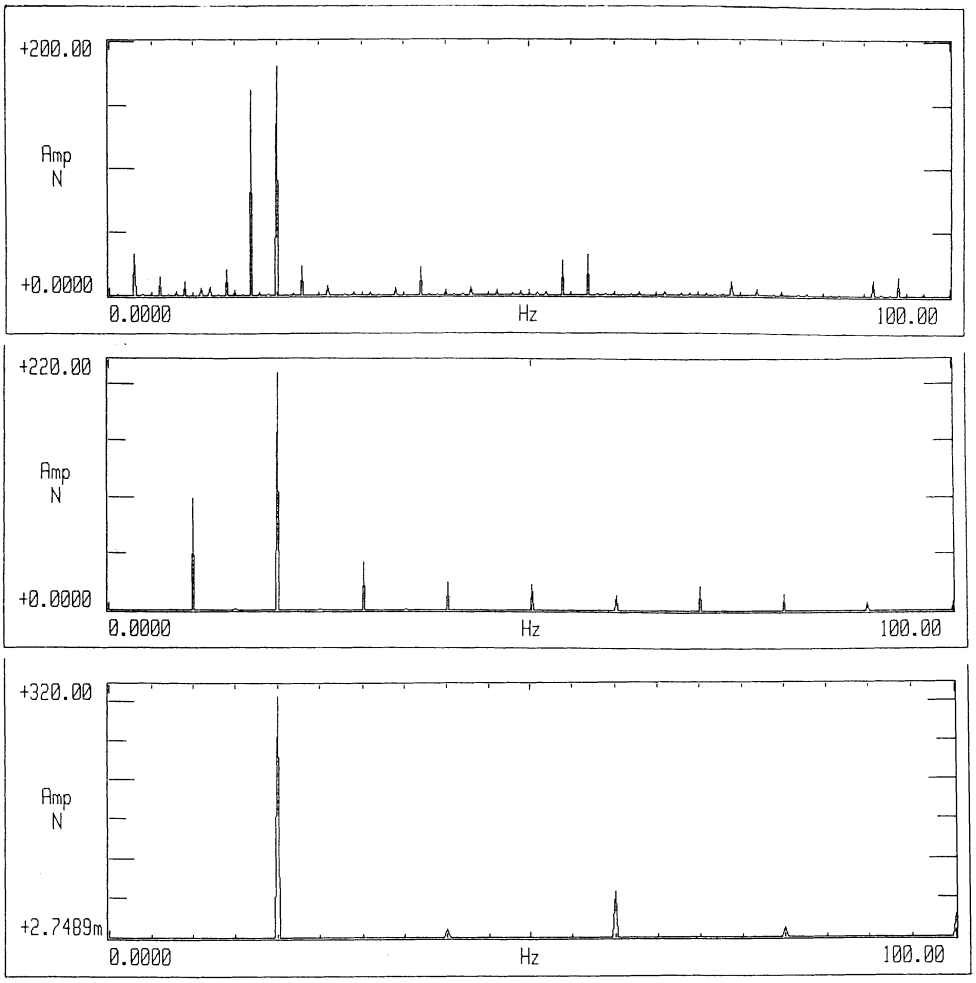

Fig. 5 Output spectrum from a non-linear system to an input of two sine waves at 20 and 17 Hz (top), 20 and 10 Hz (middle) and at 20 Hz (bottom)

3 APPARATUS

Experimental testing was carried out using an HP UNIX work-station connected to a 12 channel DIFA Scadas II data acquisition system. Data were acquired by the programmable dual filter amplifier modulus (PDFAs) and an excitation signal was generated and fired by the quadruple analogue to digital converter module (QDAC) at the front of the Scadas II. The software used to drive the system was a commercially available dynamic testing package, supplied by Leuven Measurement and Systems (LMS). Specific dedicated code was written by the author in the LMS user programmable acquisition (UPA) language to probe the damper harmonically and perform all subsequent acquisition and analysis of data.

The experimental apparatus was set up as shown in Fig. 7. The test facility consisted of a Zonic 1107 hydraulic actuator and dual-loop master controller. The base of the actuator was secured to the concrete floor. The main body of the damper was connected to the actuator head and the piston of the damper was connected via a piezoelectric force transducer to the surrounding metal structure. The dual-loop master controller was set to control the static and dynamic displacement of the actuator head. The input displacement was measured from a displacement transducer incorporated within the actuator.

3.1 Non-linearities of the actuator

Hydraulic actuators are known to be non-linear. The output from the damper therefore cannot be directly related to the defined input at the QDAC but to some distorted input from the actuator. Figure 8 shows the spectrum of a sinusoidal input signal at 10 Hz from the QDAC, from the actuator, and the output force response from the damper. The non-linearities of the actuator have introduced into the input higher order harmonics which distort the sinusoidal signal. The non-linearities of the damper will also produce harmonics in the output spectrum but, unfortunately, it is

Table 1 Frequency components produced in the output response from a non-linear system when the input consists of two sine waves at 20 and 17 Hz

Term	Frequency component (Hz)	Description
$X_1 H_1(\omega_1)$	20	
$X_2 H_1(\omega_2)$	17	
$(X_1^2/2)H_2(\omega_1, \omega_1)$	40	
$(X_1^2/2)H_2(\omega_1, -\omega_1)$	0	
$(X_1X_2/2)H_2(\omega_1, \omega_2)$	37	True component of H_2 FRF
$(X_1X_2/2)H_2(\omega_1, -\omega_2)$	3	
$(X_2^2/2)H_2(\omega_2, \omega_2)$	34	
$(X_2^2/2)H_2(\omega_2, -\omega_2)$	0	
$(X_1^3/4)H_3(\omega_1, \omega_1, \omega_1)$	60	
$(3X_1^3/4)H_3(\omega_1, \omega_1, -\omega_1)$	20	
$(X_1^2X_2/4)H_3(\omega_1, \omega_1, \omega_2)$	57	
$(X_1^2X_2/4)H_3(\omega_1, \omega_1, -\omega_2)$	23	
$(X_1^2X_2/2)H_3(\omega_1, -\omega_1, \omega_2)$	17	
$(X_1X_2^2/2)H_3(\omega_1, \omega_2, \omega_2)$	54	
$(X_1X_2^2/4)H_3(-\omega_1, \omega_2, \omega_2)$	14	
$(X_1X_2^2/2)H_3(\omega_1, \omega_2, -\omega_2)$	20	
$(X_2^3/4)H_3(\omega_2, \omega_2, \omega_2)$	51	
$(3X_2^3/4)H_3(\omega_2, \omega_2, -\omega_2)$	17	
+ higher order terms ⋮		

Table 2 Frequency components produced in the output response from a non-linear system when the input consists of two sine waves at 20 and 10 Hz

Term	Frequency component (Hz)	Description
$X_1 H_1(\omega_1)$	20	
$X_2 H_1(\omega_2)$	10	
$(X_1^2/2)H_2(\omega_1, \omega_1)$	40	
$(X_1^2/2)H_2(\omega_1, -\omega_1)$	0	
$(X_1X_2/2)H_2(\omega_1, \omega_2)$	30	True component of H_2 FRF
$(X_1X_2/2)H_2(\omega_1, -\omega_2)$	10	
$(X_2^2/2)H_2(\omega_2, \omega_2)$	20	
$(X_2^2/2)H_2(\omega_2, -\omega_2)$	0	
$(X_1^3/4)H_3(\omega_1, \omega_1, \omega_1)$	60	
$(3X_1^3/4)H_3(\omega_1, \omega_1, -\omega_1)$	20	
$(X_1^2X_2/4)H_3(\omega_1, \omega_1, \omega_2)$	50	
$(X_1^2X_2/4)H_3(\omega_1, \omega_1, -\omega_2)$	30	Additional component of H_2 FRF
$(X_1^2X_2/2)H_3(\omega_1, -\omega_1, \omega_2)$	10	
$(X_1X_2^2/2)H_3(\omega_1, \omega_2, \omega_2)$	40	
$(X_1X_2^2/4)H_3(-\omega_1, \omega_2, \omega_2)$	0	
$(X_1X_2^2/2)H_3(\omega_1, \omega_2, -\omega_2)$	20	
$(X_2^3/4)H_3(\omega_2, \omega_2, \omega_2)$	30	Additional component of H_2 FRF
$(3X_2^3/4)H_3(\omega_2, \omega_2, -\omega_2)$	10	
+ higher order terms ⋮		

Table 3 Frequency components produced in the output spectrum from a non-linear system when the input consists of a sine wave at 20 Hz

Term	Frequency component (Hz)	Description
$X_1 H_1(\omega_1)$	20	
$X_2 H_1(\omega_2)$	20	
$(X_1^2/2)H_2(\omega_1, \omega_1)$	40	Additional component of H_2 FRF
$(X_1^2/2)H_2(\omega_1, -\omega_1)$	0	
$(X_1X_2/2)H_2(\omega_1, \omega_2)$	40	True component of H_2 FRF
$(X_1X_2/2)H_2(\omega_1, -\omega_2)$	0	
$(X_2^2/2)H_2(\omega_2, \omega_2)$	40	Additional component of H_2 FRF
$(X_2^2/2)H_2(\omega_2, -\omega_2)$	0	
$(X_1^3/4)H_3(\omega_1, \omega_1, \omega_1)$	60	
$(3X_1^3/4)H_3(\omega_1, \omega_1, -\omega_1)$	20	
$(X_1^2X_2/4)H_3(\omega_1, \omega_1, \omega_2)$	60	
$(X_1^2X_2/4)H_3(\omega_1, \omega_1, -\omega_2)$	20	
$(X_1^2X_2/2)H_3(\omega_1, -\omega_1, \omega_2)$	20	
$(X_1X_2^2/2)H_3(\omega_1, \omega_2, \omega_2)$	60	
$(X_1X_2^2/4)H_3(-\omega_1, \omega_2, \omega_2)$	20	
$(X_1X_2^2/2)H_3(\omega_1, \omega_2, -\omega_2)$	20	
$(X_2^3/4)H_3(\omega_2, \omega_2, \omega_2)$	60	
$(3X_2^3/4)H_3(\omega_2, \omega_2, -\omega_2)$	20	
+ higher order terms ⋮		

impossible to determine which parts of the output harmonics are due to the damper and which parts are due to the additional input from the actuator. The actuator therefore represents an additional non-linear system in series with the damper. To minimize the effect of the actuator, the damper was tested at a low input amplitude. However, the composite HFRFs will represent the damper and actuator as a single system and are dependent on the input amplitude.

3.2 Harmonic probing software

Harmonic probing is a relatively slow method. For each frequency point in the FRF a sinusoidal input must be generated and the HFRF calculated from the input and output response spectra. Computer software was developed to automate this process using the UPA language to control the DIFA Scadas II.

For harmonic probing to be successful, the exact frequency of the input excitation must be controlled. The QDAC signal generator could only achieve discrete frequencies depending on the required time step of the signal. The QDAC clock speed had a range between 4.0 and 999.9 μs in steps of 0.1 μs. The frequency generated by the QDAC therefore may not be the actual frequency required depending on the precision of the time step.

At the beginning of the program the desired frequency range, frequency step size and input amplitude are defined

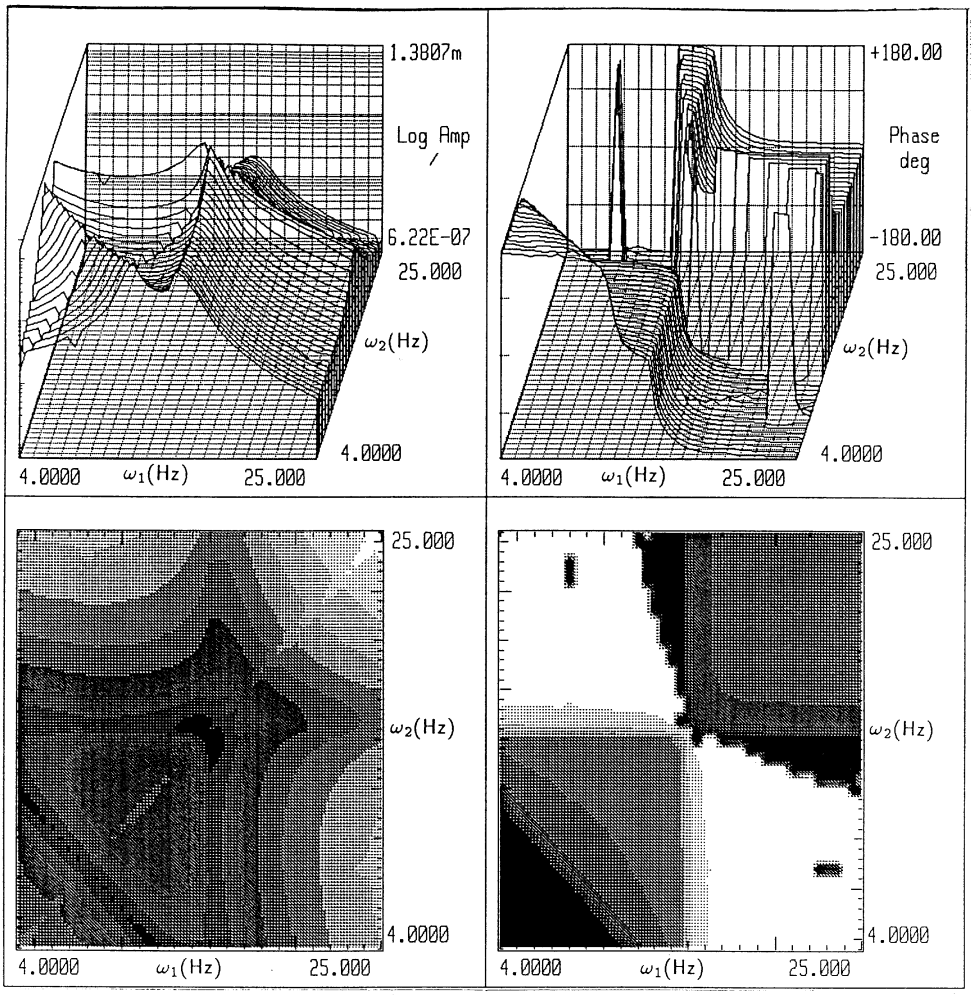

Fig. 6 The principal quadrant of the multidimensional second-order FRF $\Lambda_2(\omega_1, \omega_2)$ for the system $\ddot{y}(t) + 5\dot{y}(t) + 10^4 y(t) + 10^7 y(t)^2 + 5 \times 10^9 y(t)^3 = x(t)$, showing how degenerate terms affect the surface

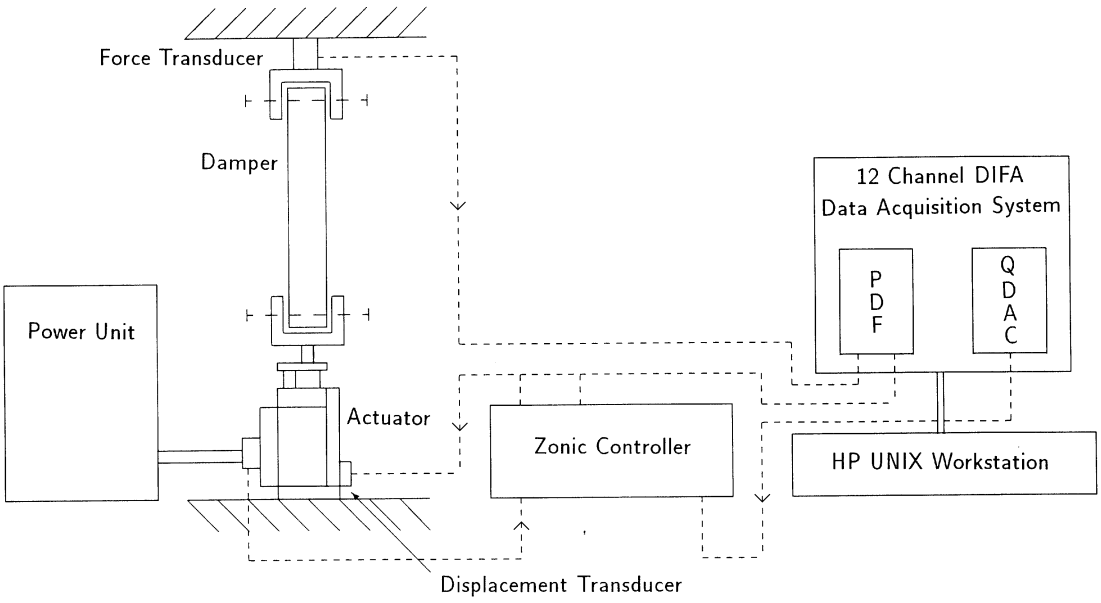

Fig. 7 Schematic diagram of the experimental apparatus

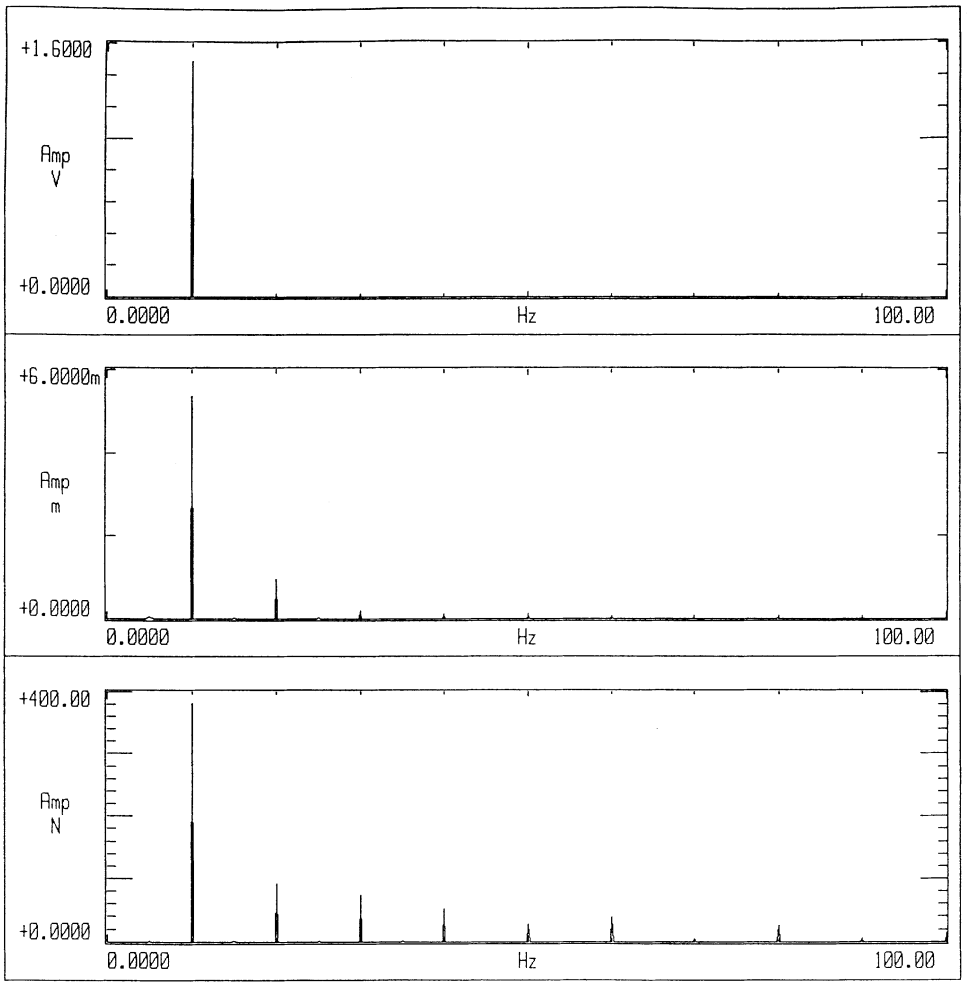

Fig. 8 Spectrum of a sinusoidal input signal: from the QDAC (upper), the signal at the actuator (middle) and the force response from the automotive damper (lower)

by the user. The software calculates the optimum frequency achievable by the QDAC for each frequency step in the FRF. The input signal is fired by the QDAC and a small time delay introduced to let all transients decay before 8192 points of input and output response time data are recorded by the PDFA acquisition modules. The sampling frequency of the PDFA modules is set equal to the sampling frequency of the input. The two recorded time responses are then Fourier transformed to obtain their spectra. By locking the PDFA and QDAC sampling frequencies, the spectra of the two responses are ensured to always contain spectral lines at the input frequency and all higher harmonics. This ensures the magnitude of the harmonics are measured accurately, a condition essential to the harmonic probing technique. The HFRFs are calculated from the spectra information and stored before the frequency is stepped and the process repeated. A complete description of the software can be found in reference (**7**).

The software was validated on an electronic circuit. The circuit represented a 'well-behaved' non-linear SDOF system and its behaviour was well documented in reference (**8**). The circuit also avoided many of the practical problems of structural testing. The signals into and out of the circuit were voltages, there was no need for an electrodynamic shaker, and the response signals did not require conditioning by charge amplifiers.

Figure 9 shows the principal diagonals of the first three composite HFRFs in terms of receptance for the circuit between 10.0 and 200.0 Hz, with a frequency step of 1.0 Hz and an input amplitude of 1.0 V peak. The first-order composite FRF contains a resonant frequency at 150.0 Hz and at low frequency the magnitude asymptotes to 0.2, giving a linear stiffness coefficient of $k_1 = 5.0$. The second-order composite FRF contains the fundamental resonance at 150.0 Hz and a secondary resonance at 75.0 Hz, half the fundamental. At low frequency the magnitude of the second-order FRF asymptotes to 3.0×10^{-3}, giving a quadratic stiffness of $k_2 = 3.75 \times 10^{-1}$. The third-order composite FRF contains a resonance at 50.0 Hz, a third of the fundamental. However,

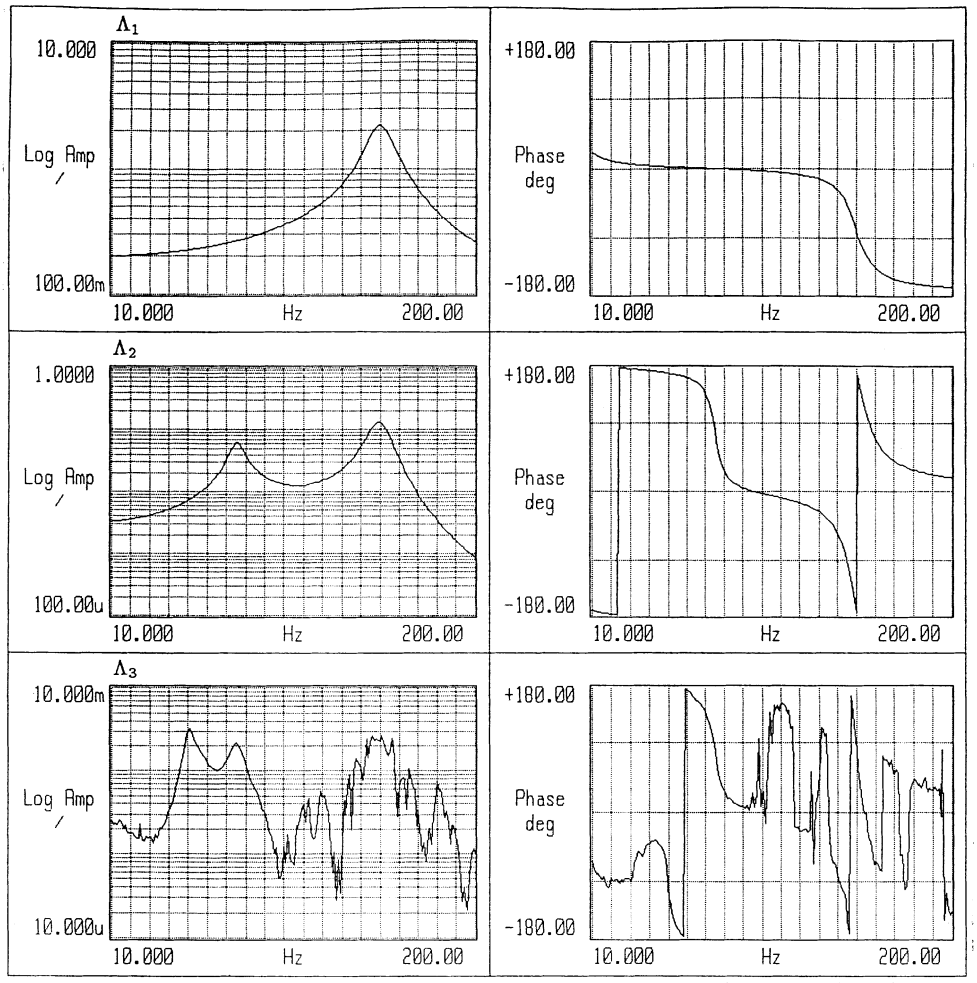

Fig. 9 Principal diagonals of the first-, second- and third-order composite FRFs in terms of receptance for the circuit at an input of 1 V peak

the quality of this FRF is poor between the ranges of 10.0–30.0 Hz and 100.0–200.0 Hz. It was assumed that the circuit contained only a small cubic stiffness, and, at low input amplitudes, the third harmonic is indistinguishable from the noise floor. To ensure this assumption was correct and not an error in the program, a further test was completed with the input amplitude increased to 3.0 V peak. Figure 10 shows the resulting composite HFRFs. The first- and second-order composite FRFs remain unchanged, apart from the fundamental resonance being skewed to a lower frequency, an effect consistent with a system whose non-linearity is dominated by a quadratic term and excited at high input amplitudes. The quality of the third-order composite FRF has improved and three resonances can be seen in the magnitude, although above 170.0 Hz the FRF is still poor. At low frequency the magnitude asymptotes to 1.0×10^{-4}, giving a cubic stiffness of $k_3 = -6.25 \times 10^{-3}$.

Table 4 compares the circuit's parameters obtained from the harmonic probing software to the results obtained by Storer, using direct parameter estimation by singular value decomposition in reference (**8**). The circuit parameters obtained from the software compared well with those obtained in reference (**8**), and the second- and third-order composite FRFs contained secondary and tertiary resonances at 75.0 Hz and 50.0 Hz. The software was therefore considered successful.

Figures 11 and 12 show the principal quadrant of the second- and third-order composite multidimensional FRFs for the circuit over the frequency range 10.0–200.0 Hz, in terms of magnitude and phase with corresponding contour plots. The amplitude of the input signal remained at 3.0 V peak but the frequency step was increased to 2.0 Hz. A ridge appears on the second-order composite FRF along the line where $\omega_1 + \omega_2 = 150.0$ Hz and two ridges appear on the third-order composite FRF along the lines where $2\omega_1 + \omega_2 = 150.0$ Hz and $\omega_1 + \omega_2 = 150.0$ Hz. These results are consistent with HFRF theory, and therefore the software developed to probe multidimensional HFRFs was considered successful.

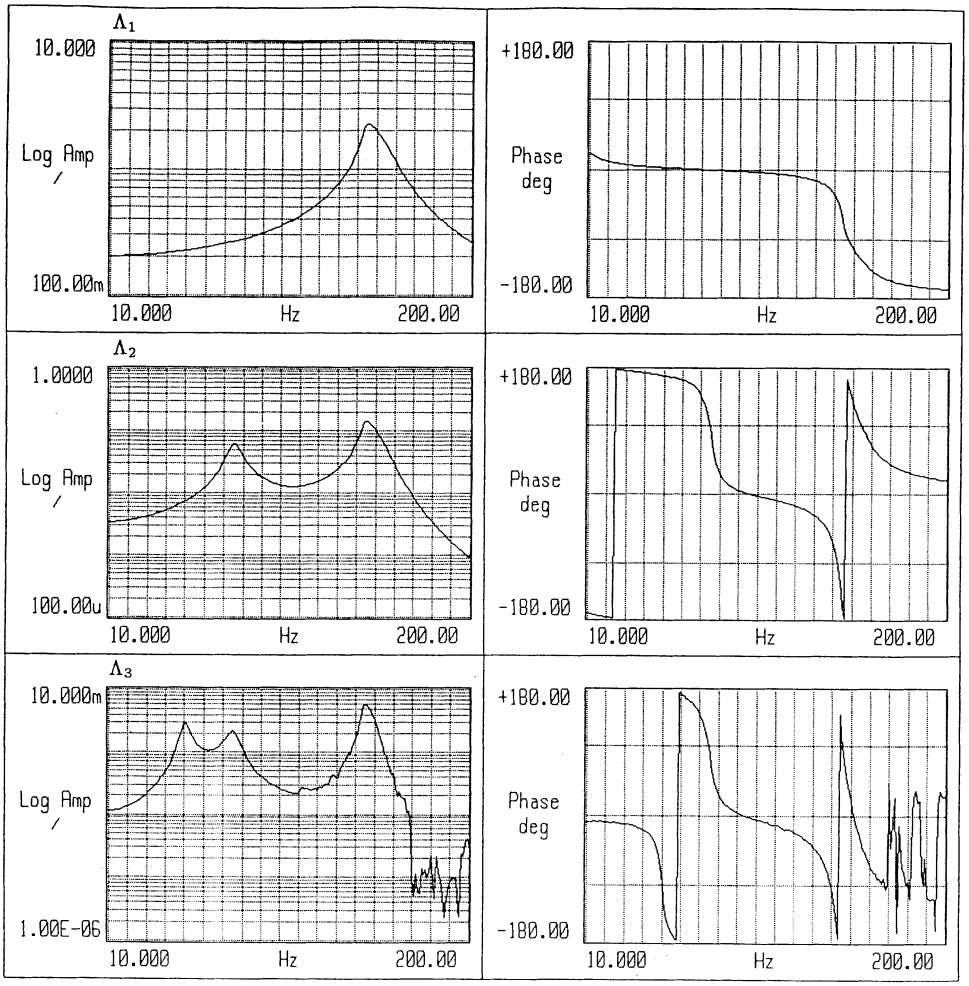

Fig. 10 Principal diagonals of the first-, second- and third-order composite FRFs in terms of receptance for the circuit at an input of 3 V peak

Table 4 Comparison of the parameters obtained for the electronic circuit by harmonic probing software and Storer

Parameter	Harmonic probing	Storer
m	5.54×10^{-6}	5.63×10^{-6}
c	1.1×10^{-3}	4.7×10^{-4}
k_1	5.0	5.0
k_2	3.75×10^{-1}	7.25×10^{-2}
k_3	-6.25×10^{-3}	-9.60×10^{-3}

4 EXPERIMENTAL PROCEDURE

The damping force of an automotive damper is predominantly dependent on velocity. Defining FRFs for an automotive damper in terms of output force/input velocity reduces the form of the FRF to a simple expression dependent only on the damping coefficient of the damper. Unfortunately, it was difficult to measure the input velocity from the actuator accurately; accelerometers produced a signal that was corrupted with pump noise from the hydraulic power unit. However, a high-quality input displacement signal could be recorded directly from the displacement transducer incorporated within the actuator. All FRFs for the automotive damper were therefore defined in terms of force output/input displacement (dynamic stiffness).

The actuator's hydraulic oil was allowed to warm to its operating temperature before the beginning of any tests. The principal diagonals of the first three composite HFRFs were obtained over the frequency range 2.0–50.0 Hz, with a 0.5 Hz resolution. A thermocouple was attached to the outer casing of the damper to allow the temperature of the damping oil to be monitored and recorded. A time delay of 2 min was introduced between each frequency step to allow the oil to cool and ensure the temperature remained relatively constant over the test. The HFRFs were obtained at an input voltage of 0.5 V. The input voltage level of 0.5 V produced a force–velocity diagram that displayed the

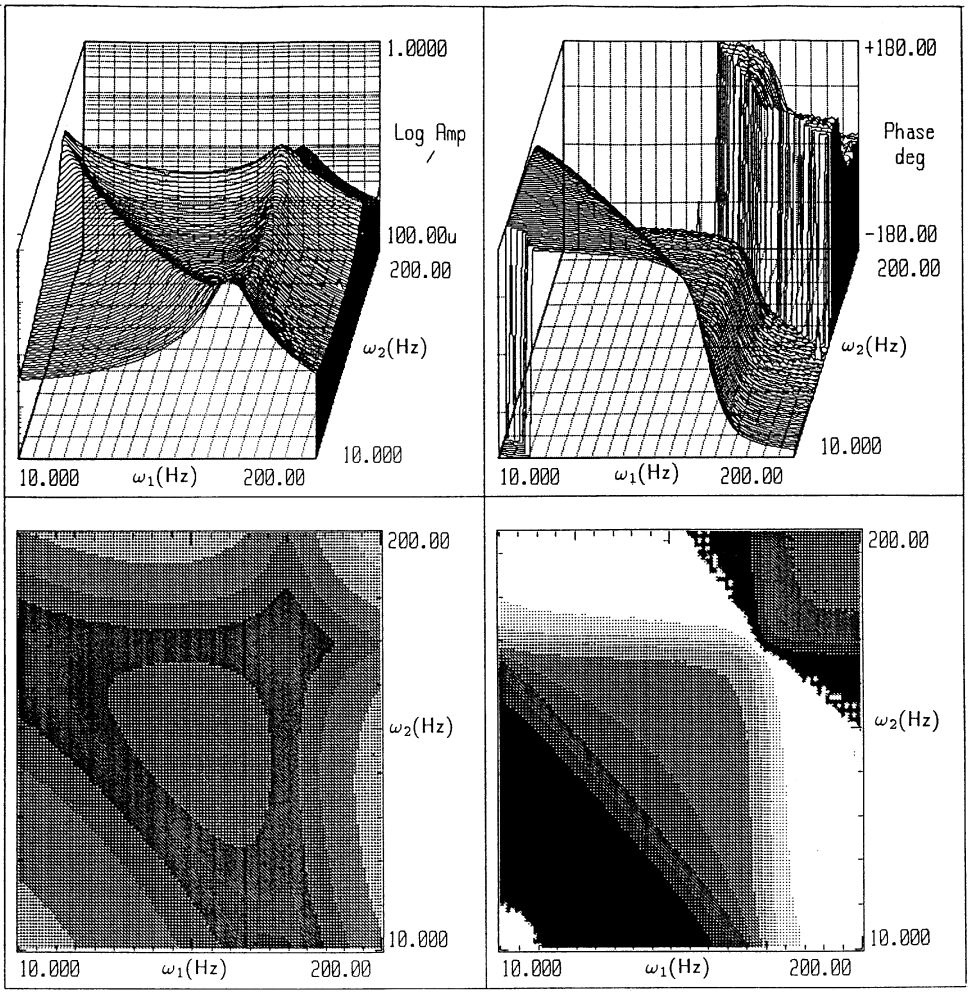

Fig. 11 Principal quadrant of the second-order composite FRF $A_2(\omega_1, \omega_2)$ in terms of receptance for the circuit at an input of 3 V peak

cleanest characteristics of the damper without introducing large amounts of hysteresis from the damper or additional non-linear effects from the actuator.

The multidimensional second- and third-order composite HFRFs were acquired for the damper over the frequency range 2.0–50.0 Hz with an input amplitude of 0.5 V. The frequency step was increased to 1.0 Hz to reduce the amount of time taken to complete the HFRFs.

5 RESULTS

Figure 13 shows the principal diagonal of the first three composite HFRFs for the damper, in terms of magnitude and phase. The HFRFs show the damper has no resonant conditions within the frequency range tested and therefore no preferred frequencies for energy transfer as in a resonant structure.

The force output from the damper is considered to be represented by

$$f(t) = c_1\dot{y}(t) + c_2\dot{y}(t)^2 + c_3\dot{y}(t)^3 + \cdots + c_n\dot{y}(t)^n \tag{29}$$

where $c_1, c_2, c_3, \ldots, c_n$ are the linear and non-linear damping coefficients. For a harmonic input the velocity can be replaced in terms of displacement and equation (29) becomes

$$f(t) = ic_1\omega_1 Y\,\mathrm{e}^{\mathrm{i}\omega_1 t} - c_2\omega_1^2 Y^2\,\mathrm{e}^{\mathrm{i}2\omega_1 t} - ic_3\omega_1^3 Y^3\,\mathrm{e}^{\mathrm{i}3\omega_1 t} + \cdots + c_n i^n \omega_1^n Y^n\,\mathrm{e}^{\mathrm{i}n\omega_1 t} \tag{30}$$

Assuming a pure harmonic input, a Volterra series representation of the force output can be derived from equation (6) as

$$f(t) = YH_1(\omega_1)\,\mathrm{e}^{\mathrm{i}\omega_1 t} + Y^2 H_2(\omega_1, \omega_1)\,\mathrm{e}^{\mathrm{i}2\omega_1 t} + Y^3 H_3(\omega_1, \omega_1, \omega_1)\,\mathrm{e}^{\mathrm{i}3\omega_1 t} + \cdots + Y^n H_n(\omega_1, \ldots, \omega_1)\,\mathrm{e}^{\mathrm{i}n\omega_1 t} \tag{31}$$

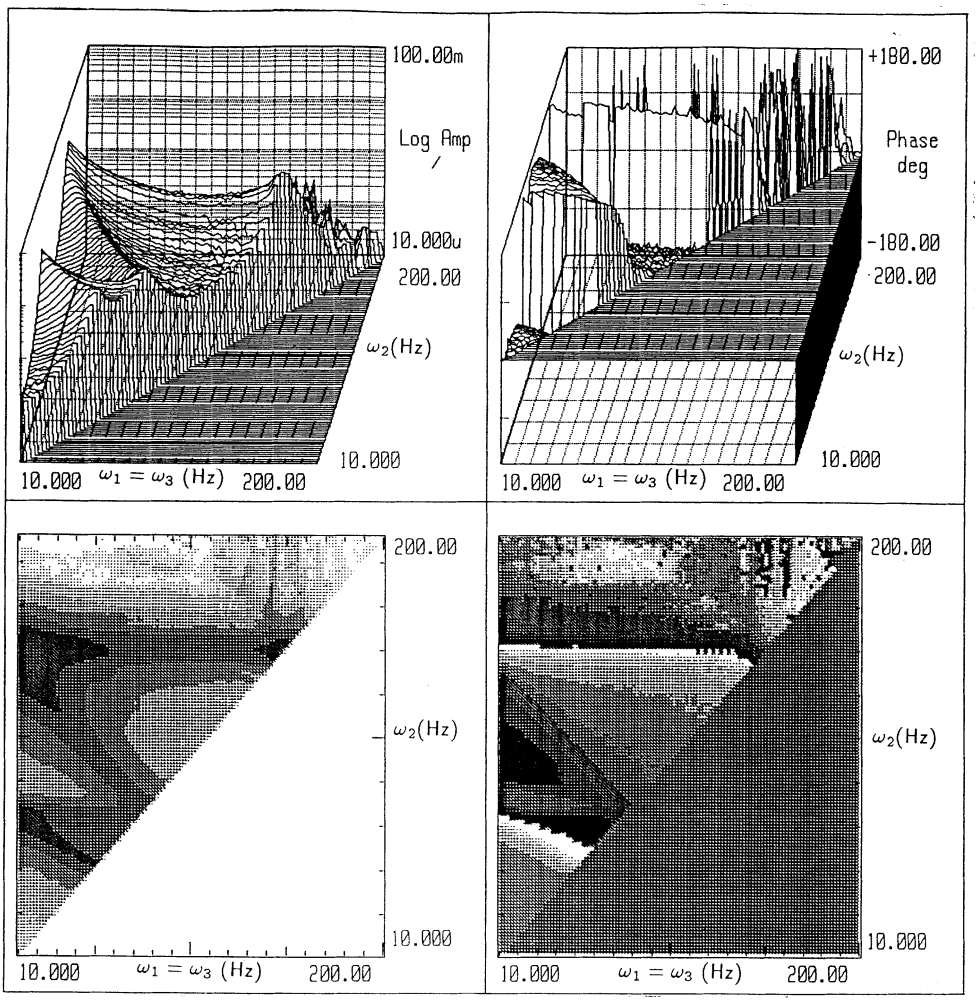

Fig. 12 Principal quadrant of the third-order composite FRF $A_3(\omega_1, \omega_2, \omega_1)$ in terms of receptance for the circuit at an input of 3 V peak

Substituting equation (30) into equation (31) and equating coefficients of $e^{i\omega t}$, $e^{i2\omega t}$ and $e^{i3\omega t}$ gives expressions for the principal diagonal of the first three HFRFs in terms of dynamic stiffness.

$$H_1(\omega) = ic_1\omega \tag{32}$$

$$H_2(\omega, \omega) = -c_2\omega^2 \tag{33}$$

$$H_3(\omega, \omega, \omega) = -ic_3\omega^3 \tag{34}$$

The magnitude of the first-order FRF increases linearly with frequency, the gradient of this increase is the linear damping coefficient c_1. The 'i' term indicates the fundamental input and output harmonics are in quadrature. The magnitude of the second-order FRF is quadratic with frequency, and the magnitude of the third-order FRF is cubic with frequency. The 'i' term again indicates the third harmonic in the output is in quadrature with the fundamental input harmonic.

By continuing to equate coefficients of higher order, expressions can be obtained for the principal diagonal of all HFRFs to order n.

$$H_n(\omega, \ldots, \omega_n) = i^n c_n \omega^n \tag{35}$$

By dividing the magnitudes of the HFRFs in Fig. 13 at each frequency step, by ω, ω^2 and ω^3 respectively, the linear and non-linear damping coefficients can be plotted, as shown in Fig. 14. The damping coefficients asymptote to a constant at high frequencies, the values of which are given in Table 5.

The sign of the coefficients is determined from the phase of their corresponding HFRF. The first-order FRF has an approximately constant phase at 90°. The expression for the first-order FRF in equation (32) is therefore positive and hence c_1 is positive. The phase of the second-order FRF is not constant but appears to drift close to 0°. If a constant phase of zero is assumed, the expression for the second-order FRF in equation (33) is positive and hence c_2 is

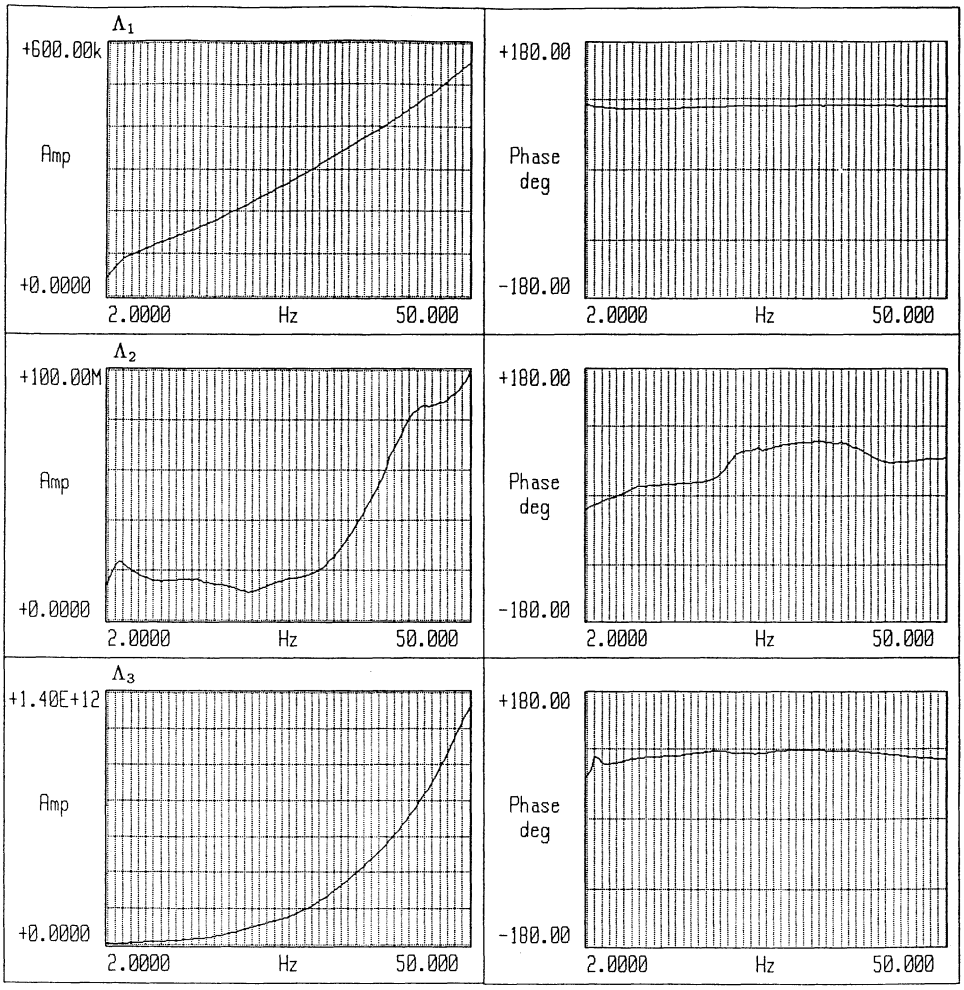

Fig. 13 Principal diagonal of the first-, second- and third-order composite FRFs for the damper

negative. The phase of the third-order FRF is approximately constant at 90°, the expression for the third-order FRF in equation (34) is therefore positive and hence c_3 is negative.

The damping coefficients from the HFRFs were used to model the damper's behaviour. To assess their accuracy, a force–velocity diagram was obtained from data generated by the model, and compared to a force–velocity diagram from experimental data using a 2–50 Hz band-limited random input at 0.5 V. Figure 15 shows the force–velocity diagram from the experimental data and Fig. 16 shows a section through this force–velocity diagram at zero displacement. The two diagrams clearly show the damper's characteristics are dominated by a cubic softening behaviour. This is consistent with the large negative third-order coefficient determined from the HFRFs.

Figure 17 compares the sectioned force–velocity diagram from the model with the sectioned force–velocity diagram from the experimental data. The model fit is poor with a normalized mean-square error of 41.0 per cent. Figure 18 shows the contribution from each coefficient to the damping characteristics of the model. The linear coefficient is clearly too small. However, it is difficult to compare force–velocity diagrams from data obtained by random excitation at 0.5 V with model data using coefficients from harmonic probing at 0.5 V. This is because the response of the damper is dependent on the type and level of the input.

A better representation of the damper's behaviour could be obtained by fitting a polynomial model to data using a least-squares estimation. Table 6 compares the coefficients from the HFRFs with those from a third-order polynomial model fitted to the experimental data. Figure 19 compares the force–velocity diagrams from the experimental data with the least-squares model. The least-squares model has a normalized mean-square error of 4.5 per cent, significantly better than the model from the HFRFs.

The process of characterizing automotive dampers using HFRFs appears to offer little advantage over polynomial models. An improved model could be obtained by introducing coefficients of higher order by measuring the principal diagonal of the corresponding HFRF. However,

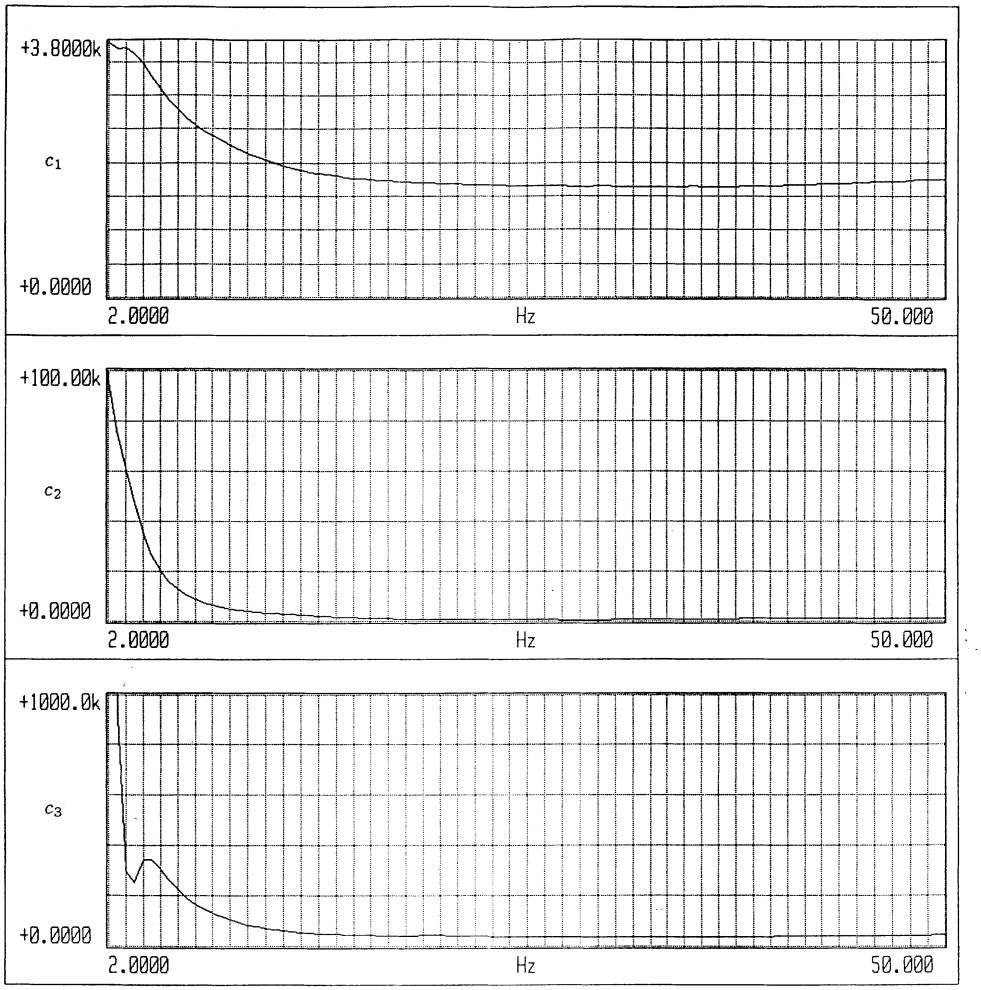

Fig. 14 Non-linear damping values for the damper

Table 5 Values of the linear and non-linear damping coefficients

Term	Damping value	Units
c_1	$1.60e+3$	$N/(m/s)$
c_2	$-8.32e+2$	$N/(m/s)^2$
c_3	$-3.85e+4$	$N/(m/s)^3$

the technique's success is limited by the inaccuracy of the coefficients, a consequence of the inability to measure the pure HFRFs and the fact that the non-linearities of the actuator distort the sinusoidal input and create additional components to the harmonics in the force output. Unfortunately, it is impossible to separate the individual components of a harmonic, hence all coefficients determined from the composite HFRFs are not general but conditional on the type and level of the input. By changing the input a new set of HFRFs and coefficients are required to characterize the damper's behaviour.

Figures 20 and 21 show the principal quadrant of the multidimensional second- and third-order FRFs, in terms of magnitude, phase and corresponding contour plots. To reduce the number of tests required to complete the multidimensional HFRFs, only half of the surfaces were obtained experimentally. The multidimensional second-order FRF was completed by mirroring the data along its axis of symmetry, the principal diagonal. Unfortunately, this technique is invalid for the third-order FRF and so only half the surface was obtained. The multidimensional HFRFs appear to offer no new information about the characteristics of the damper. The response of the multidimensional second-order FRF can be predicted by considering an input containing two harmonics. The Volterra series representation of the force output can be written from equation (6) as

$$f(t) = H_1(\omega_1)Y_1\,e^{i\omega_1 t} + H_1(\omega_2)Y_2\,e^{i\omega_2 t} + H_2(\omega_1, \omega_1)Y_1^2\,e^{i2\omega_1 t} + H_2(\omega_2, \omega_2)Y_2^2\,e^{i2\omega_2 t} + 2H_2(\omega_1, \omega_2)Y_1 Y_2\,e^{i(\omega_1+\omega_2)t} \quad (36)$$

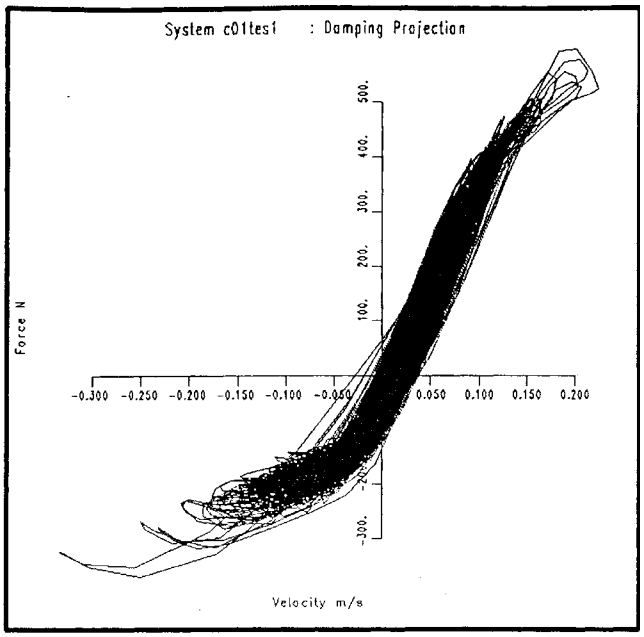

Fig. 15 Force–velocity diagram for the damper using 2–50 Hz band-limited random excitation at input voltage of 0.5 V

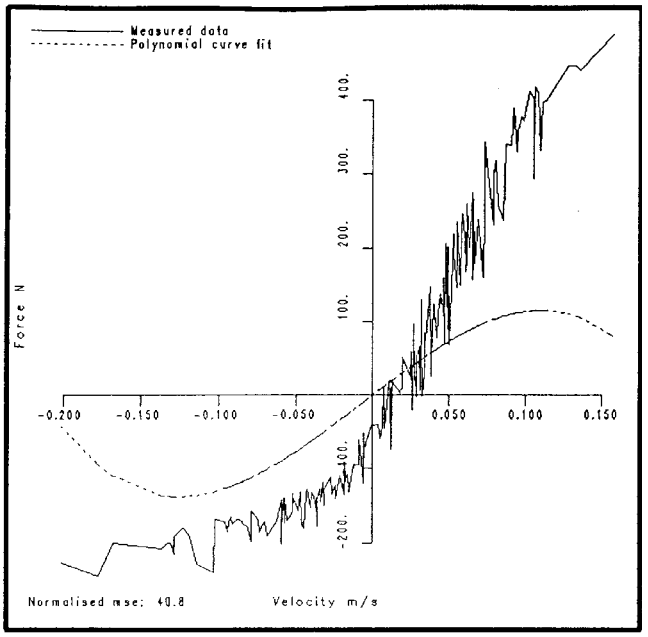

Fig. 17 Sectioned force–velocity diagram for the damper and model

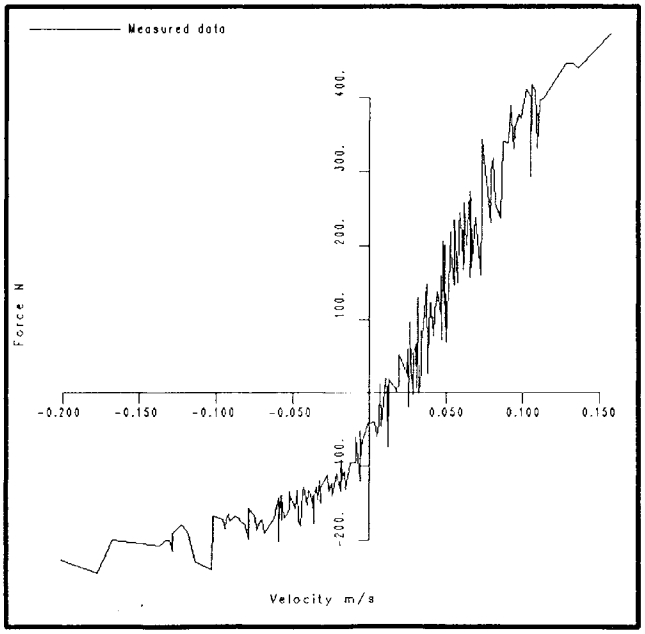

Fig. 16 Sectioned force–velocity diagram for the damper using 2–50 Hz band-limited random excitation at input voltage of 0.5 V

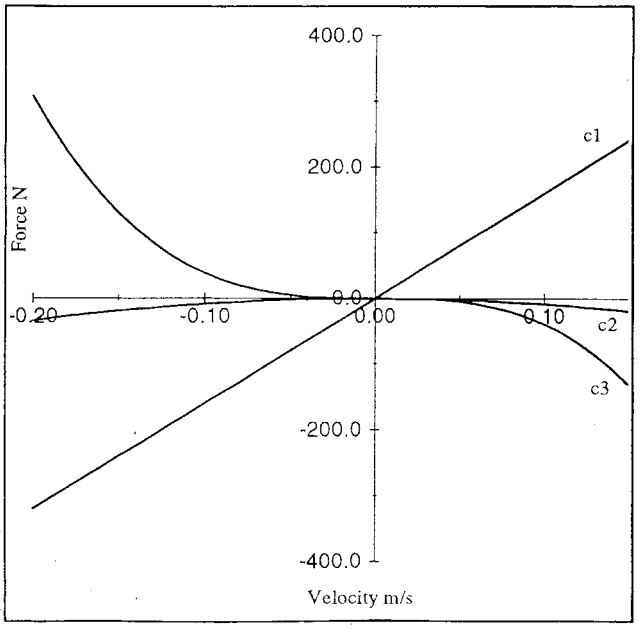

Fig. 18 Contribution to damping force from the HFRF coefficients

If the input is

$$y(t) = Y_1 e^{i\omega_1 t} + Y_2 e^{i\omega_2 t} \tag{37}$$

the velocity becomes

$$\dot{y}(t) = i\omega_1 Y_1 e^{i\omega_1 t} + i\omega_2 Y_2 e^{i\omega_2 t} \tag{38}$$

and

$$\dot{y}(t)^2 = -\omega_1^2 Y_1^2 e^{i2\omega_1 t} - 2\omega_1\omega_2 Y_1 Y_2 e^{i(\omega_1+\omega_2)t} - \omega_2^2 Y_2^2 e^{i2\omega_2 t} \tag{39}$$

Substituting equations (36), (37), (38) and (39) into

Table 6 Comparison of coefficients from a least-squares estimate and the HFRFs

Coefficient	HFRFs	Least-squares	Units
c_0		$-3.75e+1$	N
c_1	$1.60e+3$	$2.86e+3$	N/(m/s)
c_2	$-8.32e+2$	$8.93e+3$	N/(m/s)^2
c_3	$-3.85e+4$	$-9.36e+3$	N/(m/s)^3
M.S.E.	41.0	4.5	%

equation (29) and equating coefficients of $e^{i(\omega_1+\omega_2)t}$ gives

$$H_2(\omega_1, \omega_2) = -c_2\omega_1\omega_2 \tag{40}$$

The magnitude of the multidimensional second-order FRF is dependent on the multiple of the two frequencies. However, the phase in Fig. 20 appears more regular than in the principal diagonal, in areas of high frequency the phase is constant at 0°, validating the assumption that c_2 was negative.

A similar expression for the multidimensional surface of the third-order FRF can be obtained by assuming an

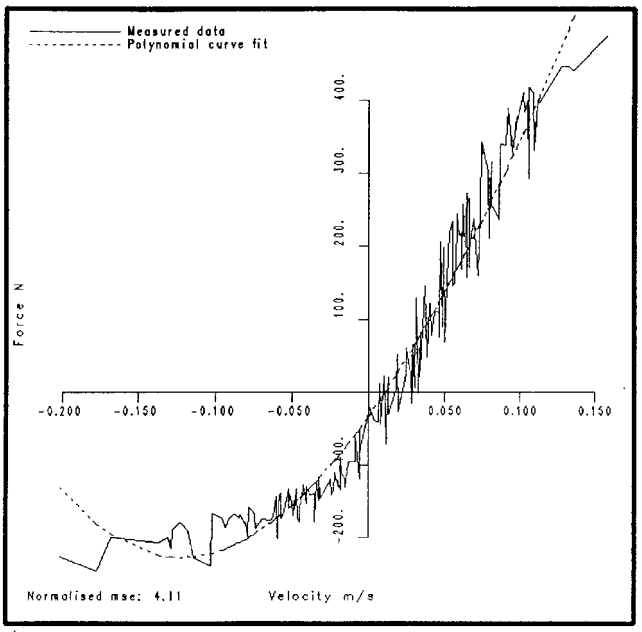

Fig. 19 Sectioned force–velocity diagram for the damper and curve fit using coefficients from the least-squares estimation

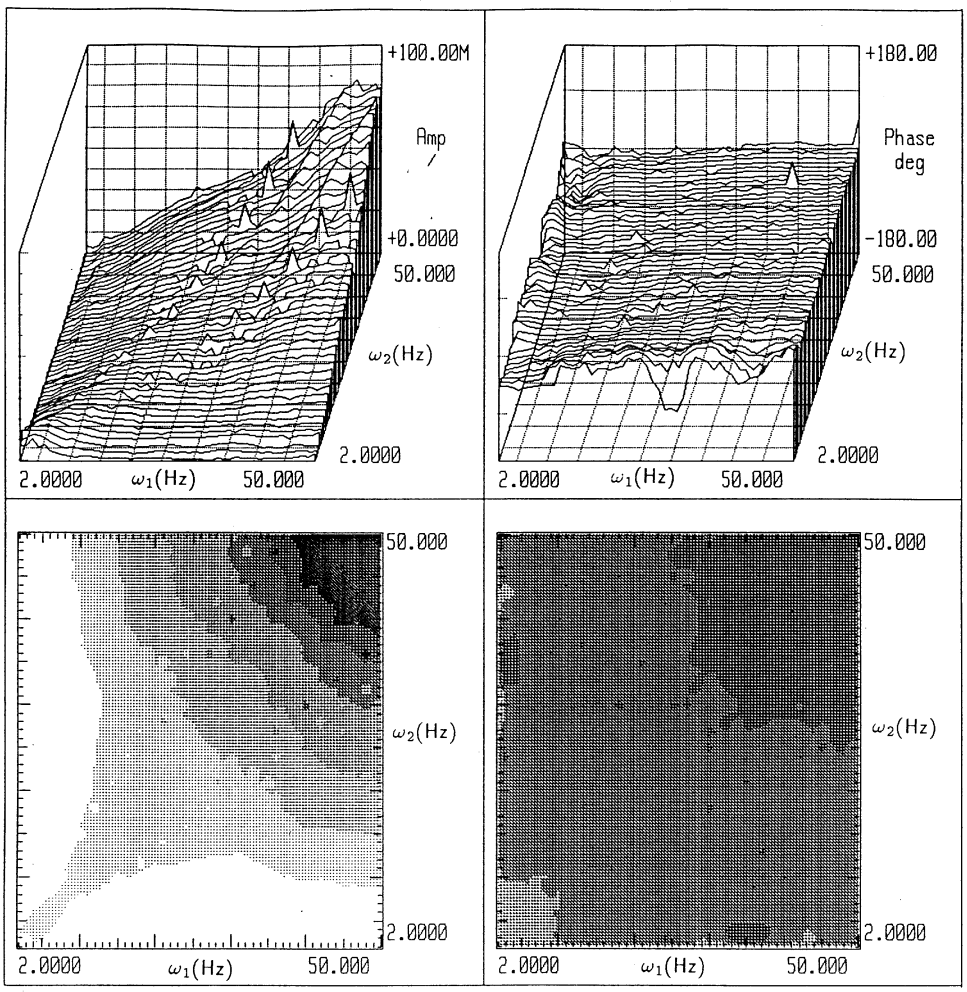

Fig. 20 Principal quadrant of the second-order composite FRF $\Lambda_2(\omega_1, \omega_2)$ for the damper

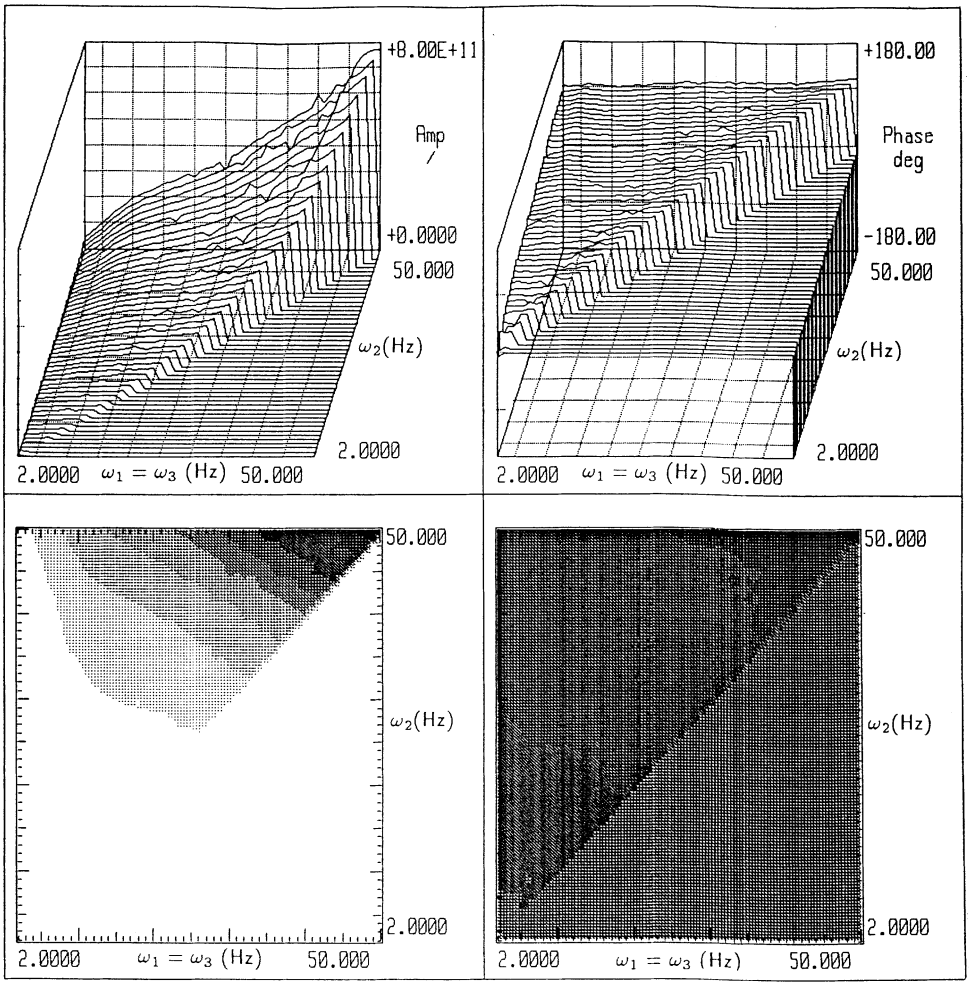

Fig. 21 Principal quadrant of the third-order FRF composite $A_3(\omega_1, \omega_2, \omega_1)$ for the damper

input of three harmonics and equating coefficients of $e^{i(\omega_1+\omega_2+\omega_3)t}$ to give

$$H_3(\omega_1, \omega_2, \omega_3) = -ic_3\omega_1\omega_2\omega_3 \tag{41}$$

The magnitude of the FRF is a multiple of the three input frequencies.

6 CONCLUSIONS

The principal diagonals of the first three composite HFRFs were successfully obtained for the automotive damper using the harmonic probing technique. The magnitude of the HFRFs contained no peaks indicating that there were no preferred frequencies for energy transfer. The HFRFs provided simple non-linear damping coefficients for the automotive damper. However, the accuracy of these coefficients was poor compared to polynomial models fitted by least-squares estimation. This was due to the inability of the technique to measure the pure HFRFs, a consequence of harmonic probing with a sine wave. This constraint, and the inability to separate the non-linear effects of the actuator from those of the damper, currently impose some limit on the use of the methodology.

The multidimensional HFRFs are considered unnecessary for characterizing the behaviour of an automotive damper. They appear to offer no useful additional information over the principal diagonals.

REFERENCES

1 **Belingarde, G.** and **Campanile, P.** Improvement of the shock absorber dynamic simulation by the restoring force mapping method. Proceedings of the 15th International Seminar on *Modal Analysis and Structural Dynamics*, Leuven, Belgium, 1990.

2 **Worden, K.** and **Tomlinson, G. R.** Parametric and nonparametric identification of Automotive Shock Absorbers. Proceedings of the 10th International Conference on *Modal Analysis*, San Diego, 1992, pp. 764–771.

3 **Worden, K.** and **Tomlinson, G. R.** Restoring force identification of shock absorbers. Research carried out under contract to Centro Ricerche FIAT (CRF), Turin, Italy, 1991.

4 **Audenino, A., Belingarde, G.** and **Garibaldi, L.** An application of the restoring force surface mapping method for the diagnostic of vehicular shock absorbers dynamic behaviour. Preprint, Dipartimento di Meccanica del Politecnico di Torino.
5 **Volterra, V.** *Theory of Functionals and Integral Equations*, 1959 (Dover Publications, New York).
6 **Bedrosian, E.** and **Rice, S. O.** The output properties of Volterra systems (nonlinear systems with memory) driven by harmonic and Gaussian inputs. *Proc. IEEE*, 1971, **59**(12), 1688–1707.
7 **Cafferty, S.** Characterisation of automotive shock absorbers using time and frequency domain techniques. PhD thesis, Department of Engineering, University of Manchester, United Kingdom, 1996.
8 **Storer, D. M.** Dynamic analysis of nonlinear structures using higher order frequency response functions. PhD thesis, Department of Engineering, University of Manchester, United Kingdom, 1991.
9 **Barrett, J. F.** The use of functionals in the analysis of nonlinear systems. *J. Electronics and Control*, 1963, **15**, 567–615.
10 **Schetzen, M.** *The Volterra and Wiener Theories of Nonlinear Systems*, 1980 (John Wiley Interscience, New York).
11 **Boyd, S., Tang, Y. S.** and **Chua, L. O.** Measuring Volterra kernels. *IEEE Trans. on Circuits and Systems*, 1983, **30**(8).